


ORIGINAL ARTICLE

NHE7 upregulation potentiates the uptake of small extracellular vesicles by enhancing maturation of macropinosomes in hepatocellular carcinoma

Yue Yao^{1,2} | Yi Xu^{1,3,4} | Liang Yu^{1,3} | Ting-Mao Xue^{1,5} | Zhi-Jie Xiao⁶ |
Pui-Chi Tin¹ | Hiu-Ling Fung¹ | Hoi-Tang Ma^{1,7} | Jing-Ping Yun⁸ |
Judy Wai Ping Yam^{1,7} 

¹Department of Pathology, School of Clinical Medicine, Li Ka Shing Faculty of Medicine, The University of Hong Kong, Hong Kong, P. R. China

²Department of Endocrinology and Metabolism, Second Affiliated Hospital of Harbin Medical University, Harbin, Heilongjing, P. R. China

³Department of Hepatopancreatobiliary Surgery, Second Affiliated Hospital of Harbin Medical University, Harbin, Heilongjing, P. R. China

⁴State Key Laboratory of Oncology in South China, Cancer Center of Sun Yat-sen University, Guangzhou, Guangdong, P. R. China

⁵Department of Hepatobiliary Surgery II, Zhujiang Hospital, Southern Medical University, Guangzhou, Guangdong, P. R. China

⁶Scientific Research Center, The Seventh Affiliated Hospital, Sun Yat-sen University, Shenzhen, Guangdong, P. R. China

⁷State Key Laboratory of Liver Research, The University of Hong Kong, Hong Kong, P. R. China

⁸Department of Pathology, Cancer Center of Sun Yat-sen University, Guangzhou, Guangdong, P. R. China

Correspondence

Judy Wai Ping Yam, Department of Pathology, 7/F Block T, Queen Mary Hospital, Pokfulam, Hong Kong, P. R. China.

Email: judyam@pathology.hku.hk

Abstract

Background: Small extracellular vesicles (sEVs) mediate intercellular communication that contributes to hepatocellular carcinoma (HCC) progression via multifaceted pathways. The success of cell entry determines the effect of sEV on recipient cells. Here, we aimed to delineate the mechanisms underlying the uptake of sEV in HCC.

Abbreviations: AF, Alexa Fluor; ANOVA, analysis of variance; ATP9A, ATPase Phospholipid Transporting 9A; BCECF-AM, 2',7'-bis-(2-carboxyethyl)-5-(and-6)-carboxyfluorescein, acetoxymethyl ester; BSA, bovine serum albumin; CCMR, Centre for Comparative Medicine Research; CRISPR, clustered regularly interspaced short palindromic repeats; CTL, ctrl; CXCR4, C-X-C Chemokine Receptor Type 4; DAPI, 4',6-diamidino-2-phenylindole; DFS, disease-free survival; DMEM, Dulbecco's Modified Eagle Medium; DMSO, dimethyl sulfoxide; Dox, doxycycline; EEA1, early endosome antigen 1; EIPA, 5-(N-ethyl-N-isopropyl)-amiloride; FBS, fetal bovine serum; FITC, fluorescein isothiocyanate; GAPDH, glyceraldehyde-3-phosphate dehydrogenase; GM130, Golgi matrix protein 130; HCC, hepatocellular carcinoma; HEPES, 4-(2-hydroxyethyl)-1-piperazineethanesulfonic acid; HPRT1, hypoxanthine phosphoribosyltransferase 1; H-score, histoscore; IAA, indole-3-acetic acid; KD, knockdown; KO, knockout; mAID, mini-auxin-inducible degron; MTT, 3-(4,5-dimethylthiazol-2-yl)-2,5-diphenyltetrazolium bromide; NHE7, Na(+)/H(+) exchanger 7; ns, non-significant; OD, optical density; OS, overall survival; PBS, phosphate-buffered saline; PCR, polymerase chain reaction; pHe, endosomal pH; pHi, intracellular pH; PKH67, Paul Karl Horan 67; Rab21, Ras-associated binding protein 21; RIPA, radioimmunoprecipitation assay; SAM, synergistic activation mediator; SEMs, standard error of the means; sEVs, small extracellular vesicles; sgRNA, single-guide RNA; shRNA, short-hairpin RNA; SLC9, solute carrier gene 9; SLICE, Seamless Ligation Cloning Extract; TCGA, The Cancer Genome Atlas; TCL, total cell lysates; TGN, trans-Golgi network; TMA, tissue microarray; TMR, tetramethyl rhodamine; TSG101, tumor susceptibility gene 101.

Yue Yao and Yi Xu contributed equally to this work.

This is an open access article under the terms of the [Creative Commons Attribution-NonCommercial-NoDerivs](https://creativecommons.org/licenses/by-nc-nd/4.0/) License, which permits use and distribution in any medium, provided the original work is properly cited, the use is non-commercial and no modifications or adaptations are made.

© 2023 The Authors. *Cancer Communications* published by John Wiley & Sons Australia, Ltd on behalf of SUN YAT-SEN UNIVERSITY CANCER CENTER.

Funding information

Natural Science Foundation of Heilongjiang Province, Grant/Award Number: LH2023H043; University Research Committee, University of Hong Kong, Grant/Award Number: 202111159009; Research Grants Council, University Grants Committee, Grant/Award Number: 17105322; Society of Hong Kong Scholars, Grant/Award Numbers: XJ2020012, 2020-036; Harbin Medical University, Grant/Award Number: HMUMIF-22008; State Key Laboratory of Oncology in South China, Grant/Award Number: HN2023-02

Methods: Macropinocytosis was examined by the ability of cells to internalize dextran and sEV. Macropinocytosis was analyzed in Na(+)/H(+) exchanger 7 (NHE7)-knockdown and -overexpressing cells. The properties of cells were studied using functional assays. pH biosensor was used to evaluate the intracellular and endosomal pH. The expression of NHE7 in patients' liver tissues was examined by immunofluorescent staining. Inducible silencing of NHE7 in established tumors was performed to reveal the therapeutic potential of targeting NHE7.

Results: The data revealed that macropinocytosis controlled the internalization of sEVs and their oncogenic effect on recipient cells. It was found that metastatic HCC cells exhibited the highest efficiency of sEV uptake relative to normal liver cells and non-metastatic HCC cells. Attenuation of macropinocytic activity by 5-(N-ethyl-N-isopropyl)-amiloride (EIPA) limited the entry of sEVs and compromised cell aggressiveness. Mechanistically, we delineated that high level of NHE7, a sodium-hydrogen exchanger, alkalized intracellular pH and acidized endosomal pH, leading to the maturation of macropinosomes. Inducible inhibition of NHE7 in established tumors developed in mice delayed tumor development and suppressed lung metastasis. Clinically, NHE7 expression was upregulated and linked to dismal prognosis of HCC.

Conclusions: This study advances the understanding that NHE7 enhances sEV uptake by macropinocytosis to promote the malignant properties of HCC cells. Inhibition of sEV uptake via macropinocytosis can be exploited as a treatment alone or in combination with conventional therapeutic approaches for HCC.

KEYWORDS

hepatocellular carcinoma, small extracellular vesicles, macropinocytosis, pH regulation, sodium-hydrogen exchanger

1 | BACKGROUND

Hepatocellular carcinoma (HCC), the major subtype of liver cancer, accounts for over 90% of cases [1]. HCC is a deadly malignancy with very limited treatment options. Although new breakthroughs have been made in systemic therapies, image-guided ablation, radiotherapy and surgical interventions in recent years, HCC remains a global health challenge.

Small extracellular vesicles (sEVs) are cell membrane-enclosed particles (50-150 nm) secreting by virtually all cells. sEVs play pivotal roles through transferring functional materials such as DNA, mRNA, microRNA, proteins and lipids to other cell types, where they modulate cellular properties and orchestrate signaling pathways [2]. In HCC, nidogen 1 in metastatic HCC cell-derived sEVs facilitate cancer cell colonization and extrahepatic metastasis via boosting angiogenesis and pulmonary endothelial permeability [3]. Polymeric immunoglobulin receptor-enriched sEVs isolated from patients with late-stage HCC pro-

mote cancer stemness, aggressiveness and metastasis [4]. Pyruvate kinase M2 derived from sEVs secreted from HCC cells induces monocyte-to-macrophage transformation and tumor microenvironment remodeling to enhance HCC aggressiveness [5]. Although much effort has been made on the functional role and underlying clinical values of sEV cargoes in HCC, how HCC cells internalize sEVs remains unexplored.

The entry pathway of sEVs is of vital importance in determining the effect of sEVs on recipient cells. Cells have been reported to internalize sEVs via different endocytic approaches, including clathrin-mediated endocytosis, caveolin-dependent internalization, macropinocytosis, phagocytosis, and lipid raft-dependent uptake [6]. Macropinocytosis is a process that extracellular fluid is incorporated into large vesicles named macropinosomes. It is tightly linked to actin cytoskeleton dynamics regulated by small guanosine triphosphatases [7]. Spontaneous occurrence at the basal level is observed, but its activation is evident in cells containing the *Ras* oncogene, leading

to enhanced nutrient internalization and subsequent promotion of tumor cell progression [8]. Previous studies have shown that cancers of the pancreas [8], prostate [9] and lung with activating *RAS* mutations [10] exhibit constitutive macropinocytosis. For sEV internalization, Costa Verdera *et al.* [11] reported that clathrin-independent endocytosis and macropinocytosis are the main pathways for HeLa cervical cancer cells to uptake sEVs derived from A431 human epidermoid carcinoma cells. Oncogenic *KRAS* has been proven to maintain Panc-1 pancreatic ductal adenocarcinoma cells with increased macropinocytic activity, which facilitates cellular uptake of sEVs [12]. Fibronectin is a cargo of hepatocyte sEVs which plays a role in sEV uptake via clathrin- and caveolin-dependent internalization and macropinocytosis by targeting hepatocytes and hepatic stellate cells [13]. In addition, vacuolar protein sorting 4 homolog A promotes the uptake of tumor suppressive microRNAs carried by sEVs into HCC cells [14]. sEV uptake is not simply a channel of intercellular communication within the tumor microenvironment but also provides insights into the design of new systems to deliver anticancer drugs into tumor cells [15].

In this work, we first assessed the macropinocytic capacity of normal liver cells, non-metastatic and metastatic HCC cells. In addition, the influence of 5-(N-ethyl-N-isopropyl)-amiloride (EIPA) as well as Na(+)/H(+) exchanger 7 (NHE7) on HCC cell macropinocytosis and progression was explored. What's more, we investigated the influence of NHE7 on promoting the maturation of macropinosomes. Mechanistically, the intracellular and endosomal pH, which controls the internalization of sEVs, regulated by NHE7 was evaluated. At last, inducible disruption of NHE7 expression alone or combining with sorafenib administration was performed on established tumors to evaluate their synergistic antitumor efficacy on HCC.

2 | MATERIALS AND METHODS

2.1 | Human specimens

Paired tumor and adjacent non-tumor liver tissues were employed for the construction of tissue microarray (TMA) which was provided by the Department of Pathology, Sun Yat-sen University Cancer Center (Guangzhou, Guangdong, China). The authorization for utilization of patients' specimens was acquired from the Institutional Review Board of The University of Hong Kong/Hospital Authority Hong Kong West Cluster (Approval number: UW 11-448, Hong Kong, China) and Sun Yat-sen University Cancer Center (Approval number: B2021-459-01, Guangzhou, Guangdong, China). The study involved

human tissues were handled following the relevant ethical guidelines.

2.2 | Cell culture

The non-metastatic human HCC cell line PLC/PRF/5 and the human embryonic kidney cell line 293FT were acquired from the American Type Culture Collection (Manassas, VA, USA). The non-metastatic human HCC cell line HLE was obtained from Japanese Collection of Research Bioresources (Ibaraki, Osaka, Japan). Two metastatic human HCC cell lines MHCC97L and MHC-CLM3 were acquired from the Cancer Institute of Fudan University (Shanghai, China). The human immortalized hepatocyte MIHA was provided by Dr. Jayanta Roy-Chowdhury (Albert Einstein College of Medicine, New York, NY, USA). The detailed information of cells used in this study is shown in Supplementary Table S1. These cells were maintained in Dulbecco's Modified Eagle Medium (DMEM; #12100, Gibco, Waltham, MA, USA) containing 10% fetal bovine serum (FBS; #10270-106, Gibco), 100 U/mL penicillin and 100 µg/mL streptomycin (#15140122, Invitrogen, Carlsbad, CA, USA). All the cells were cultured at 37°C with 5% CO₂.

2.3 | Construction of expression vectors

To construct expression vector of short-hairpin RNA (shRNA) targeting NHE7, annealed oligos of shRNA were subcloned into pLKO.1-puro vector (#8453, Addgene, Cambridge, MA, USA) via the AgeI and EcoRI sites. Clustered regularly interspaced short palindromic repeats (CRISPR) synergistic activation mediator (SAM) was performed to overexpress NHE7 in HCC cells. Annealed oligos of single-guide RNA (sgRNA) of NHE7 was subcloned into sgRNA (MS2)_{zeo} backbone (#61427, Addgene) via the BsmBI site. To employ mini-auxin-inducible degron (mAID) technology that allows rapid degradation of NHE7, sgRNA of NHE7 (CR1 and CR2) was also subcloned into pX300 via the BbsI site (#42230, Addgene) to create the *NHE7*-mAID-KO cells. cDNA of NHE7 was amplified using cDNA of MHCC97L cells with primers NHE7-cDNA-F and NHE7-cDNA-R. The polymerase chain reaction (PCR) product was subcloned into *NheI*- and *BamHI*-digested pUHD-SB-c-mAID/Hyg [16] using Seamless Ligation Cloning Extract (SLICE) cloning method [17] to construct *NHE7*-mAID in pUHD-SB-mAID/Hyg vector. The oligos are listed in Supplementary Table S2. For all cloning, the ligation mix was transformed in *E. coli* DH5α (#FEREC0112, Thermo Fisher Scientific, Waltham, MA, USA), which was subsequently plated onto ampicillin-containing agar plates. A single

clone was inoculated in Luria-Bertani broth (#12795084, Thermo Fisher Scientific) and maintained at 37°C with vigorous agitation. A miniprep kit (#27106, Qiagen, Hilden, Nordrhein-Westfalen, Germany) was used to purify DNA plasmids. Sanger sequencing was used to confirm presence of *NHE7* oligo sequence in the vector.

2.4 | Establishment of stable *NHE7*-knockdown and -overexpressing cells

Stable *NHE7*-knockdown cells (*NHE7*-KD) and non-targeting control cells (*CTL*-KD) were constructed in MHCCLM3 and MHCC97L cell lines. To generate lentiviral particles, human embryonal kidney cell line HEK293FT was co-transfected with pLKO.1-*NHE7*-KD vector, LentiPac HIV mix (#LT002, GeneCopoeia, Rockville, MD, USA) and EndoFectin Lenti transfection reagent (#EF002, GeneCopoeia). The medium containing viral particles were collected and filtered. The medium along with polybrene (#TR-1003, Sigma-Aldrich, Saint Louis, MO, USA) were utilized to treat the HCC cells. Puromycin (#54041, Merck Millipore, Billerica, MA, USA) was applied for selection. CRISPR SAM was performed to establish *NHE7*-overexpressing cells (*NHE7*-SAM) and control cells (*CTL*-SAM) in HLE and PLC/PRF/5 cell lines. Three vectors, Lenti dCAS-VP64_Blast (#61425, Addgene), LentiMPH v2 (#89308, Addgene) and sgRNA (MS2)_zeo, with or without sgRNA of *NHE7* were transduced into cells. Afterwards, the cells were selected by a combination of blasticidin (#A1113903, Gibco), hygromycin B (#10687010, Gibco) and zeocin (#R25001, Thermo Fisher Scientific). The luciferase-labeled MHCC97L cell line was used to create *NHE7*-mAID-KO cells. MHCC97L cells were transduced with pX300 expressing *NHE7* CR1 and CR2, *NHE7*mAID in pUHD-SB-c-mAID/Hyg, pSBbi-TIR1/Pur and pCMV(CAT)T7-SB100 (Sleeping Beauty transposase). Transduced cells were enriched with hygromycin B and puromycin for two weeks as previously described [16].

2.5 | Extraction and validation of sEVs

Cells were cultured in DMEM containing sEV-depleted FBS for 72 h. Then, the supernatants were harvested and subjected to collect sEVs using differential centrifugation method as we described before [3]. The sEVs were preserved in filtered phosphate-buffered saline (PBS), and the Bradford method (#5000006, Bio-Rad Laboratories, Hercules, CA, USA) was utilized to assess the protein concentration. The size range of sEVs was analyzed by ZetaView (Particle Metrix GmbH, Meerbusch, NRW, Ger-

many). The protein lysate of sEVs was assessed for sEV molecular markers by immunoblotting.

2.6 | Immunogold labeling of sEVs

The resuspended sEV pellet was deposited on formvar carbon-coated nickel grids. After rinsing twice with PBS, the grids were placed onto blocking buffer containing 1% bovine serum albumin (BSA, #A-420-250, Goldbio, St Louis, MO, USA). Blocked grids were then treated with 15 µg/mL CD63 antibody (#ab134045, Abcam, Cambridge, MA, USA). At last, the grids were rinsed 3 times with blocking buffer prior to incubating with 6-nm gold-labeled secondary antibody (#ab41498, Abcam). After air-dried, uranyl acetate (#23631, Ladd Research, Essex Junction, VT, USA) was used to stain the grids. Finally, the grids were visualized using a transmission electron microscope (FEI Company, Hillsboro, OR, USA).

2.7 | Paul Karl Horan 67 (PKH67) labeling of sEVs

PKH67 Membrane Dye Labeling Kit (#PKH67GL, Sigma-Aldrich) was used to label sEVs with green fluorescence to track the localization of sEVs. Briefly, sEVs were resuspended in provided diluent C. PKH67 reagent was added to diluent C prior to mixing with sEVs. The mixtures were supplied with 1% BSA to eliminate the excess dye, and ultrafiltered using 100 kDa Amicon Ultra-15 Centrifugal Units (#UFC910024, Merck Millipore) at 3,000 × g for 30 min at 4°C. Subsequently, the samples were resuspended in PBS and harvested by ultracentrifugation.

2.8 | Uptake assay

High-molecular weight dextran (70 kDa) is a well-recognized indicator for macropinocytosis [18]. The cells were subjected to starvation by using serum-free medium for 16 h prior to assessing the endocytic activity for tetramethyl rhodamine (TMR)-dextran (#D1818, Invitrogen). Macropinosomes were labelled by TMR-dextran dissolved in DMEM and then incubated for 0.5 h at 37°C. To determine the internalization of PKH67-sEVs by cells, 5 × 10⁴ cells were treated with 2.5 µg of PKH67-sEVs in DMEM for 2 h. To inhibit macropinocytosis, cells were pretreated with vehicle (methanol; #MA-1291-2500, Anaqua Global International, Cleveland, OH, USA) or different concentrations of EIPA (#A3085, Sigma-Aldrich) for 30 min prior to incubation with TMR-dextran or PKH67-sEVs. After coincubation, the cells were washed

five times, fixed with paraformaldehyde (sc-281692, Santa Cruz Biotechnology, Dallas, TX, USA), treated with 4',6-diamidino-2-phenylindole (DAPI; #D9542, Sigma-Aldrich) and observed by using an LSM900 confocal microscope (Carl Zeiss, Oberkochen, BW, Germany). ImageJ (National Institutes of Health, Bethesda, MD, USA) was used to analyze the images. Total particle per cell area was evaluated from at least five fields. At least 100 cells per experiment were analyzed.

2.9 | Cell viability assessment

HCC cell viability was evaluated by 3-(4,5-dimethylthiazol-2-yl)-2,5-diphenyltetrazolium bromide (MTT; #475989, Sigma-Aldrich) experiment. MHCCLM3 or MHCC97L cells (1×10^5) were treated with either vehicle or EIPA for 30 min followed by adding 15 μ g of sEVs. After coincubation for 72 h, the cells were collected and counted. One thousand treated cells per well were seeded in 96-well dishes in triplicates. Ten μ L of MTT (5 mg/mL) were supplied to each well, and the plates were maintained at 37°C for 4 h. The absorbance was detected at 570 nm after the addition of 50 μ L of dimethyl sulfoxide (DMSO; #D2650, Sigma-Aldrich). The same EIPA and sEV treatment was applied to colony formation, migration and invasion assays below.

2.10 | Colony forming assay

sEV-pretreated cells (1×10^3) were planted in a 2.5 cm plate in triplicate and cultured for 14 days at 37°C. After fixed with 4% paraformaldehyde and stained with 0.5% crystal violet (#46364, Sigma-Aldrich), the colonies were photographed and counted by ImageJ.

2.11 | Transwell assay

Cell migratory and invasive potentials were measured using Transwell® Permeable Support assay (#353097, Corning, Corning, NY, USA). For migration assessment, HCC cells in DMEM were seeded in the upper compartment, while the bottom well was supplied with culturing medium containing 10% FBS and 1:1,000 hepatocyte growth factor (#H9661, Sigma-Aldrich) which acts as a chemo-attractant. After incubation for 16–24 h, the cells passed through the membrane were fixed, stained, photographed, and finally quantified by ImageJ. For invasion assay, Matrigel (#354234, Corning) was used to coat transwells prior to performing invasion assay. The other steps were identical to that of cell migration assay.

2.12 | Subcutaneous injection assay

All animal experiments were conducted under the research protocol authorized by Committee of the Use of Live Animals in Teaching and Research, The University of Hong Kong (Approval number: 5925-21). All the mice were raised in specific pathogen-free laboratory of Centre for Comparative Medicine Research (CCMR) of the University of Hong Kong. For subcutaneous xenograft model, 2×10^6 MHCCLM3 cells with 15 μ g of MHCCLM3-sEVs in the presence of vehicle or 5 mg/kg of EIPA were co-injected into the flank of 4–6 weeks old male BALB/cAnN-nu mice (CCMR). The major axis and minor axis of the tumors were measured every 5 or 6 days. Tumor volume was calculated as $0.5 \times (\text{major axis}) \times (\text{minor axis})^2$ [19]. Humanitarian euthanasia should be carried out in advance when the tumor diameter reached over 15 mm or tumor burden exceeded 10% of the mouse body weight. At the end of experiments, the mice were euthanized after intraperitoneal anesthesia with ketamine and xylazine.

2.13 | Co-treatment with doxycycline, indole-3-acetic acid and sorafenib in a mouse model

Luciferase-labeled parental or *NHE7*-mAID-KO MHCC97L cells were subcutaneously inoculated into 4–6 weeks old male BALB/cAnN-nu mice. When the tumor volume reached around $90 \pm 10 \text{ mm}^3$, mice bearing tumors were randomized for treatment with DMSO in water (100 μ L/day; oral gavage) or indole-3-acetic acid (IAA; 25 $\text{mg} \cdot \text{kg}^{-1} \cdot \text{day}^{-1}$, oral gavage; #I5148, Sigma-Aldrich) with or without sorafenib (30 $\text{mg} \cdot \text{kg}^{-1} \cdot \text{day}^{-1}$, oral gavage; #S8599, LC Laboratories, Woburn, MA, USA). For doxycycline (Dox) administration, Dox (#HY-N0565B, MedChemExpress, Monmouth Junction, NJ, USA) was supplied to the drinking water (2 mg/mL of Dox and 5% sucrose). Mice in the other groups were given drinking water containing 5% sucrose. The tumor volume of all groups was monitored every 3 days. Animals were humanely euthanized if the tumor diameter exceeded 12 mm, tumor burden exceeded 10% of the mouse body weight, or at the planned endpoint of the study. To acquire a tumor seed for liver orthotopic implantation, luciferase-labeled parental or *NHE7*-mAID-KO MHCC97L cells was subcutaneously inoculated into the flanks of 4–6 weeks old male BALB/cAnN-nu mice. After two weeks, the tumors were harvested and cut into pieces to insert into the liver capsule for successive orthotopic implantation in BALB/cAnN-nu mice (6–8 weeks old, male). The same treatment described above was administered for

4 weeks. Six weeks after liver orthotopic implantation, bioluminescence images were acquired and quantified by an In Vivo Imaging System (PerkinElmer, Waltham, MA, USA). The liver and lung tissues of the mice were used for histological analysis. When the mice were in poor general condition such as rapid weight loss of more than 15%, the mice would be euthanized after intraperitoneal anesthesia with ketamine and xylazine.

2.14 | Frozen tissues

Detection of macropinosomes in tissues was performed as described elsewhere [20]. Fresh subcutaneous tumors were cut into pieces and inoculated with 150 μ L of 4 mg/mL 70 kDa fluorescein isothiocyanate (FITC)-dextran (#D1822, Invitrogen). The tissue fragments were immersed in 250 μ L of FITC-dextran for 15 min in the dark prior to rinsing twice in PBS. Afterwards, an optimal cutting temperature compound (#4583, Sakura Finetek, Torrance, CA, USA) in a prelabeled cryomold was used for embedding the tissue. The frozen sections were dyed with DAPI and subsequently incubated with 1.6 μ mol/L Alexa Fluor™ 568 phalloidin (#A12380, Invitrogen) for 30 min. Images of 5 randomly selected fields were obtained using an LSM900 confocal microscope and analyzed for fluorescent signals.

2.15 | Multiplex immunofluorescence

Multiplex immunofluorescence was performed on TMA of paired HCC and adjacent non-tumor tissues. Informed consent from patients was obtained. Detailed optimization of the multiplex panel was performed as the reference [21]. Antibodies used were validated using conventional immunohistochemistry. NHE7 (1:15; HPA048938, Sigma-Aldrich)-Opal 520 (PerkinElmer) and Ras-associated binding protein 21 (Rab21; 1:100; sc-81917, Santa Cruz Biotechnology)-Opal 570 (PerkinElmer) were included in the multiplex panel. The slide was scanned by Perkin Elmer Vectra (PerkinElmer). The spectrally unmixed component images were reconstructed and exported for further analysis using inForm software (PerkinElmer). The histoscore (H-score) was calculated by multiplying the score of intensity by the percentage of positively stained cells. H-score was in the range of 0 to 300.

2.16 | Quantitative PCR

Total RNA was isolated with RNAiso Plus (#9108, Takara Bio, Shiga, Japan). The RNA was reversely transcribed

to cDNA using SuperScript VILO MasterMix (#11754250, Invitrogen). Glyceraldehyde-3-phosphate dehydrogenase (*GAPDH*) or hypoxanthine phosphoribosyltransferase 1 (*HPRT1*) was used as an internal control. The quantitative PCR assays were conducted using an SYBR Green kit (#A25742, Thermo Fisher Scientific). The sequences of related primers are shown in Supplementary Table S2.

2.17 | Immunoblotting assay

Proteins were extracted using radioimmunoprecipitation assay (RIPA; #89901, Thermo Fisher Scientific) buffer added with protease inhibitor (#05892970001, Roche, Basel, Kanton Basel, Switzerland) and phosphatase inhibitor (#04906837001, Roche). The Bradford method was utilized to quantify the concentrations of protein samples. The extracted protein was subjected to sodium dodecyl sulphate-polyacrylamide gel electrophoresis and transferred onto a polyvinylidene fluoride membrane (#IPVH00010, Merck Millipore). Western blotting was carried out using anti-NHE7 (1:1,000; #BMP043, Medical & Biological Laboratories, Nagoya, Japan), anti-Rab21 (1:1,000; #sc-81917, Santa Cruz Biotechnology) and anti- β -actin antibodies (1:5,000; #A5316, Sigma-Aldrich). β -actin was included as a loading control. ECL™ reagent (#RPN2106, GE Healthcare, Chicago, IL, USA) was utilized to observe the chemiluminescent signals. Chemiluminescence was detected using an Amersham™ Imager 680 system (Amersham, Chicago, IL, USA).

2.18 | Immunofluorescence assay

Cells were seeded onto a coverslip, and fixed with 4% paraformaldehyde. After rinsing, the cells were permeabilized with 0.1% Triton X-100 (#22686, USB Corporation, Cleveland, OH, USA) before incubating with blocking buffer (5% BSA in PBS). Primary antibodies against NHE7 (1:100; #PA5-61843, Invitrogen), early endosome antigen 1 (1:100; #ab70521, EEA1, Abcam), Rab7 (1:100; #95746, Cell Signaling Technology, Danvers, MA, USA), Rab11a (1:100; #STJ140068, St John's Laboratory, London, UK), Rab21 (1:100; #sc-81917, Santa Cruz Biotechnology), or Golgin-97 (1:100; #A21270, Invitrogen) was used to treat the cells. After rinsing in PBS, cells were maintained in secondary antibodies tagged with Alexa Fluor™ 488 or 568 (Invitrogen). Cell nuclei were stained with DAPI, and coverslips were mounted onto slides (Vector Laboratories, Burlingame, CA, USA). An LSM900 confocal microscope was used to capture images.

2.19 | Intracellular pH measurements and pH recovery measurements

Intracellular pH (pHi) values were determined by fluorescence spectroscopy using a pH-sensitive fluorescent probe 2',7'-bis-(2-carboxyethyl)-5-(and-6)-carboxyfluorescein, acetoxymethyl ester (BCECF-AM; #B1170, Invitrogen) [22]. Cells were maintained in 5 $\mu\text{mol/L}$ BCECF-AM at 37°C for 15 min. Nigericin is an ionophore that allows equilibration of intracellular pH with extracellular pH. Calibration was conducted by utilizing a high-potassium buffer supplemented with 10 $\mu\text{mol/L}$ nigericin at a pH range of 6.5–8.5. The BCECF-AM fluorescence intensity levels were measured with excitation wavelengths at 490 nm and 440 nm and an emission wavelength at 535 nm. The 490/440 nm fluorescence ratio was then converted to pHi values. To measure Na^+/H^+ exchange activity, an intracellular acid load test was carried out using the NH_4Cl -prepulse experiment [23, 24]. The 490/440 nm fluorescence ratios were measured for 40 cycles at 20-s intervals. Cells were first maintained in 4-(2-hydroxyethyl)-1-piperazineethanesulfonic acid (#15630080, HEPES; Gibco) for 4 cycles, exposed to 20 mmol/L NH_4Cl in HEPES buffer for 8 cycles, and incubated again in HEPES buffer for another 28 cycles. pHi recovery (ΔpHi) during the last 28 cycles was analyzed by subtracting the pHi value measured during exposure to NH_4Cl from the pHi values measured at 1-minute intervals during recovery for the last 28 cycles, and Na^+/H^+ exchange activity was calculated as $\Delta\text{pHi}/\Delta t$. At least 1×10^4 cells per replicate were scored.

2.20 | Endosomal pH measurements

Cells were starved in DMEM without FBS at 37°C for 0.5 h prior to treating with fluorescein and tetramethylrhodamine-coupled dextran (#D1951, Invitrogen) at 37°C for another 30 min. pH-sensitive fluorescein was used as a pH biosensor, and pH-insensitive tetramethylrhodamine was included as an internal standard for endosomal pH (pHe) measurement. Ice-cold serum-free DMEM and PBS was applied to remove the external dextran. Cells were pelleted and resuspended in PBS with or without 500 mmol/L monensin. Calibration was performed using a high-potassium buffer supplemented with 10 $\mu\text{mol/L}$ nigericin at a pH range of 5.0–7.0. The fluorescence intensity of endocytosed dextran was detected in 1×10^4 cells by flow cytometry (BD Biosciences, Franklin Lake, NJ, USA), and the ratio of fluorescein to tetramethylrhodamine in the cell population was recorded [25].

2.21 | Bioinformatics analysis

The Cancer Genome Atlas (TCGA) database (<https://www.cancer.gov/ccg/research/genome-sequencing/tcga>) was utilized to analyze the expression profiles of NHE7 between HCC tumor tissues and adjacent non-tumor tissues. Furthermore, the evaluation encompassed disease-free survival (DFS) and overall survival (OS) following treatment, comparing patients with high NHE7 expression to patients with low NHE7 expression in the top 30% percentile [26].

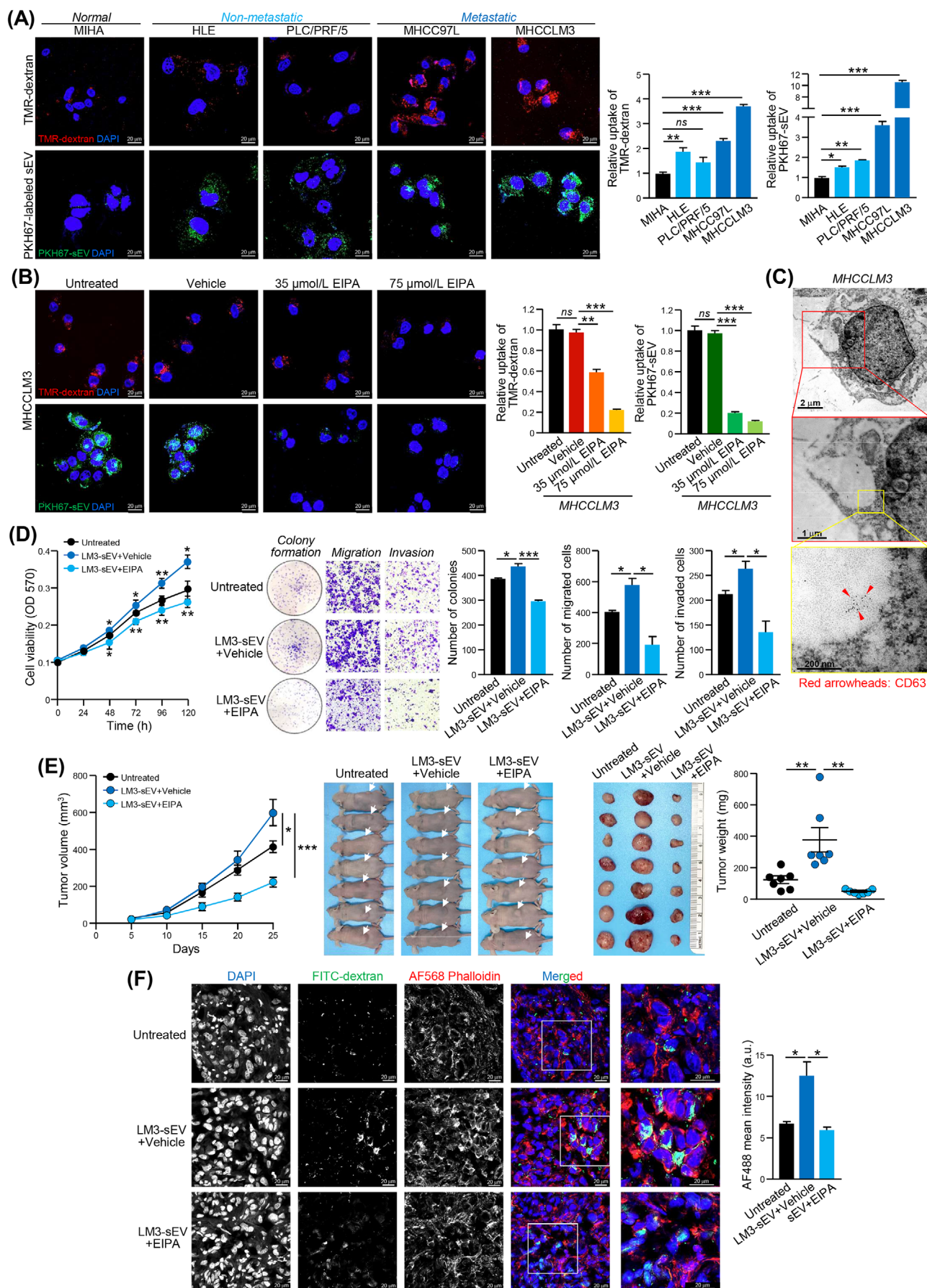
2.22 | Statistical analysis

Values are shown as the means \pm standard error of the means (SEMs). Data were analyzed via one-way analysis of variance (ANOVA) or Student's *t*-test using GraphPad Prism V8.3.0 (GraphPad, San Diego, CA, USA). $P < 0.05$ was regarded as statistical significance.

3 | RESULTS

3.1 | Metastatic HCC cells displayed enhanced macropinocytosis

To evaluate and compare macropinocytosis among normal hepatocyte (MIHA), non-metastatic HCC cells (HLE and PLC/PRF/5) and metastatic HCC cells (MHCC97L and MHCCLM3), a macropinocytosis uptake experiment using 70 kDa TMR-dextran as macropinosome marker was performed (Figure 1A). Compared to MIHA cells, HCC cells displayed an increased level of TMR-dextran uptake, with metastatic cells exhibiting the highest uptake efficiency. The uptake of PKH67-labeled sEVs (PKH67-sEVs) derived from metastatic HCC cells by normal and HCC cells was also evaluated. sEVs were isolated from HCC cells, and their identity, size and morphology were characterized (Supplementary Figure S1). Intriguingly, we observed a trend in sEV uptake similar to the observed trend in TMR-dextran uptake (Figure 1A). This observation prompted us to investigate whether the rapid uptake of sEVs by metastatic HCC cells is mediated by enhanced macropinocytosis. MHCCLM3 and MHCC97L cells were treated with EIPA, which has been proven to decrease macropinocytic activity without affecting other endocytic approaches [8, 27]. Cells were pretreated with a non-toxic concentration of EIPA (Supplementary Figure S2) and were then incubated with TMR-dextran or PKH67-sEVs. The results showed that EIPA diminished the uptake of TMR-dextran and PKH67-sEVs by both cell lines when



compared to cells treated with vehicle (Figure 1B and Supplementary Figure S3A). We further evaluated the macropinocytic activity of metastatic HCC cells using sEVs derived from a non-metastatic HCC cell line. EIPA dramatically reduced PKH67-sEV signals in cells (Supplementary Figure S3B), which was comparable to how it affected sEVs derived from metastatic HCC cells. It was also noted that the internalized TMR-dextran and PKH67-sEVs were highly co-localized in HCC cells. The uptake of dextran and sEVs and their co-localization were significantly reduced in cells treated with EIPA (Supplementary Figure S3C). Representative electron micrographs revealed that macropinosomes were generated from sites of membrane ruffling, and CD63 immunogold labelled sEVs were internalized and localized in the macropinosome (Figure 1C). Collectively, the above findings demonstrated that macropinocytosis mediates the uptake of sEVs by metastatic HCC cells.

3.2 | Inhibition of macropinocytosis hindered the promoting activity of HCC sEVs

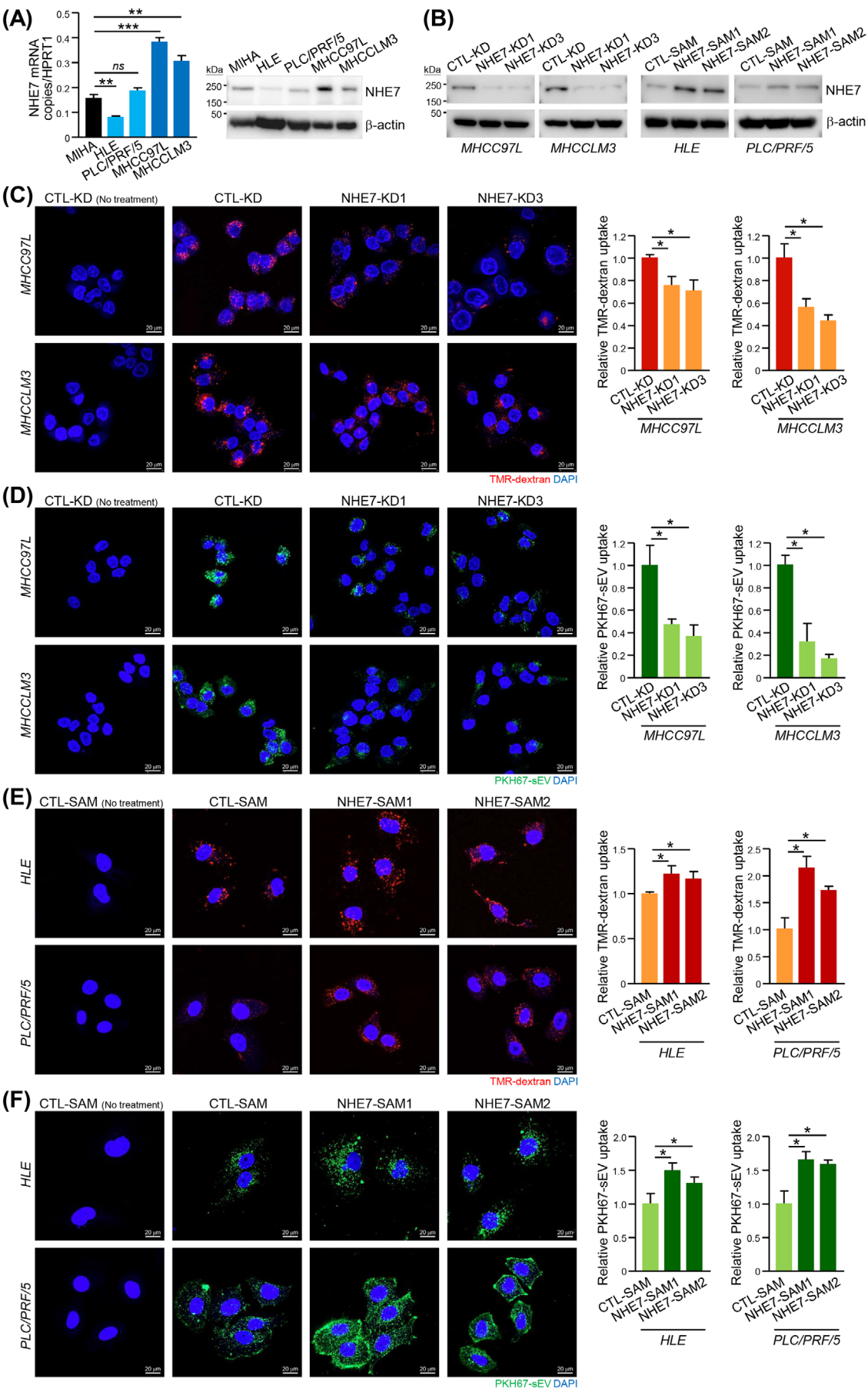
sEVs secreted from HCC cells have been demonstrated to significantly augment both the growth and aggressiveness of hepatocytes and HCC cells [3]. We then examined whether the uptake of sEVs mediated by macropinocytosis influences the oncogenic proclivity of sEVs in recipient cells. sEVs derived from MHCCLM3 cells (MHCCLM3-sEVs) significantly enhanced the proliferative, colony-forming, migratory and invasive capacities of MHCCLM3 cells, while this promoting effect was blocked when cells were treated with EIPA (Figure 1D). Simi-

lar blockade of the promoting effect of sEVs by EIPA was observed in MHCC97L cells (Supplementary Figure S3D-E). In a subcutaneous tumor xenograft model established with MHCCLM3 cells, co-injection of MHCCLM3-sEVs enhanced tumor development when compared to that in the untreated group, while this enhancement in terms of tumor volume and weight was reduced by EIPA treatment (Figure 1E). Tumor tissues harvested from the mice co-treated with MHCCLM3-sEVs and EIPA exhibited a significant suppression in macropinocytic internalization of FITC-dextran than that in mice co-treated with MHCCLM3-sEVs and DMSO (Figure 1F). Collectively, these results indicated that blocking macropinocytic uptake using EIPA strikingly prevents the promoting activity of sEVs derived from metastatic HCC cells.

3.3 | NHE7 was a potential regulator of macropinocytosis in HCC cells

To delineate the molecular basis of the enhanced macropinocytosis in metastatic HCC, we sought to determine whether Na⁺/H⁺ exchangers encoded by NHE/solute carrier gene 9 (SLC9) gene family members, which are targets of EIPA [28, 29], could be the key regulators of macropinocytosis in HCC cells. The expression of NHE1, NHE6, NHE7 and NHE9 in MIHA cells and HCC cell lines was assessed. Among all examined NHE family members, only NHE7 was significantly upregulated in MHCC97L and MHCCLM3 cells (Figure 2A and Supplementary Figure S4), which correlates with enhanced macropinocytosis in metastatic cells. To determine whether NHE7 could facilitate macropinocytosis in HCC cells, MHCC97L and MHCCLM3 clones with stable

FIGURE 1 Metastatic HCC cells exhibit enhanced sEV uptake by macropinocytosis, and blockade of macropinocytosis inhibits sEV-induced tumor growth. (A) Visualization and quantification of macropinosomes in a normal liver cell line (MIHA), non-metastatic HCC cell lines (HLE and PLC/PRF/5) and metastatic HCC cell lines (MHCC97L and MHCCLM3). Macropinocytosis uptake assay using TMR-dextran (red) as a marker of macropinosomes (*upper*) and PKH67-sEV (green; *bottom*). Nuclei were stained with DAPI (blue). (B) Macropinocytosis uptake assay using TMR-dextran and PKH67-sEV in MHCCLM3 cells pretreated with vehicle and different concentrations (35 or 75 μ mol/L) of EIPA. Cells were stained with DAPI. Total particle per cell area was evaluated from at least five fields. At least 100 cells per experiment were analyzed. The fluorescent signal intensity was quantified and normalized to the respective control cells. (C) Representative electron micrographs of sEVs subjected to immunogold labeling using anti-CD63 antibody followed by secondary antibody conjugated to 6-nm gold-labeled particles in MHCCLM3 cells. (D) The proliferation of vehicle- or 35 μ mol/L EIPA-pretreated MHCCLM3 cells incubated with sEVs was evaluated by MTT assay (*left*). MHCCLM3 cells treated with sEVs and EIPA were subjected to colony formation, migration and invasion assays. Representative images of fixed and crystal violet-stained cell colonies and migrated and invaded cells are shown (*middle*) and quantified (*right*). (E) Subcutaneous injection of MHCCLM3 cells co-injected with or without sEVs and vehicle (methanol) or EIPA (n = 7 per group). Tumor volume was monitored regularly (*left*). Image of whole mice (*middle*) and excised tumors obtained (*right*) at the end of the experiment. Tumors were weighed. (F) Representative images of frozen sections of FITC-dextran (green)-injected tumor xenografts stained with phalloidin (red) and DAPI (blue). The intensity of FITC-dextran in 5 randomly selected fields was quantified. Data are presented as the means \pm SEMs of n = 3 independent experiments. * P < 0.05; ** P < 0.01; *** P < 0.001. Abbreviations: AF, Alexa Fluor; DAPI, 4',6-diamidino-2-phenylindole; EIPA, 5-(N-ethyl-N-isopropyl)-amiloride; FITC, fluorescein isothiocyanate; HCC, hepatocellular carcinoma; MTT, 3-(4,5-dimethylthiazol-2-yl)-2,5-diphenyltetrazolium bromide; ns, non-significant; OD, optical density; PKH67: Paul Karl Horan 67; SEMs, standard error of the means; sEV, small extracellular vesicle; TMR, tetramethyl rhodamine.



NHE7 knockdown and HLE and PLC/PRF/5 clones with stable NHE7 overexpression were established (Figure 2B and Supplementary Figure S5). NHE7-knockdown cells (NHE7-KD1 and NHE7-KD3) displayed diminished uptake of TMR-dextran and PKH67-sEVs compared to CTL-KD control cells (Figure 2C-D). In contrast, the uptake of TMR-dextran and PKH67-sEVs was elevated in NHE7-overexpressing cells (NHE7-SAM1 and NHE7-SAM2) compared to the respective CTL-SAM control cells (Figure 2E-F). These data suggested that NHE7 is a promoter of macropinocytosis in HCC cells.

3.4 | NHE7 regulated macropinocytosis and determined the sEV-induced malignant properties of recipient cells

We further investigated whether recipient HCC cells with NHE7 knockdown showed alleviation of malignant properties induced by the uptake of sEVs. Both MHCC97L and MHCCLM3 CTL-KD cells treated with sEVs showed increased malignant behaviors compared with the non-sEV-treated control group in the colony forming and transwell assays. However, the enhanced malignant properties induced by sEVs were abrogated in NHE7-KD1 and NHE7-KD3 cells (Supplementary Figure S6). The in vitro results were also substantiated in a subcutaneous xenograft assay in which sEV-induced tumor development was markedly delayed in the NHE7-KD1 and NHE7-KD3 groups compared to the CTL-KD group (Figure 3A-B). The macropinocytic uptake of FITC-dextran was attenuated in NHE7-knockdown cells compared to control cells (Figure 3C). Conversely, NHE7-SAM1 and NHE7-SAM2 HLE and PLC/PRF/5 cells were demonstrated to have enhanced malignant properties induced by sEVs compared to CTL-SAM control cells (Supplementary Figure S7). In the animal study, NHE7-overexpressing cells co-injected with sEVs showed accelerated tumor development compared to the respective control cells (Figure 3D-E). Tumors

formed from NHE7-SAM1 and NHE7-SAM2 cells had a marked increase in the macropinocytic uptake of FITC-dextran compared to that of CTL-SAM cells (Figure 3F). These data suggested that NHE7 facilitates macropinocytosis, which determines the effect of sEV uptake on the properties of recipient cells.

3.5 | NHE7 promoted the maturation of macropinosomes

NHE7 has been recognized as a unique Na^+/H^+ exchanger which dynamically cycles among the trans-Golgi network (TGN), endosomes and plasma membrane [30]. In MHCC97L and MHCCLM3 cells, in which NHE7 was upregulated and had more efficient macropinocytosis than normal liver cells, only a small part of NHE7 fluorescence fell in the area of EEA1, Rab7 or Golgin-97 (Figure 4A), which are markers for early endosomes [31], late endosomes [32] and TGN [33], respectively. NHE7 was partially co-localized with Rab11a and prominently co-localized with Rab21 (Figure 4A), which are markers for recycling endosomes [32] and mature macropinosomes [34], respectively. In view of the localization of NHE7 at recycling endosomes and mature macropinosomes, we investigated whether NHE7 affects the localization and expression levels of the Rab11a and Rab21 proteins. Notably, the co-localization of NHE7 with Rab11a and Rab11a expression were not altered in NHE7-KD MHCC97L cells (Supplementary Figure S8), suggesting that NHE7 knockdown did not affect recycling of remnant NHE7-positive endosomes to the plasma membrane. Strikingly, we observed dramatic reductions in the co-localization of NHE7 with Rab21 and Rab21 expression in NHE7-KD MHCC97L cells (Figure 4B-C), whereas NHE7-SAM HLE cells exhibited a higher degree of co-localization of NHE7 with Rab21-positive macropinosomes and an elevated level of Rab21 expression (Figure 4D-E), pointing to the function of NHE7 in the maturation of macropinosomes.

FIGURE 2 NHE7 functions as a regulator of macropinocytosis in HCC cells. (A) The mRNA and protein levels of NHE7 in MIHA cells and various HCC cell lines were measured by PCR and western blotting, respectively. (B) Immunoblots showing the expression of NHE7 in MHCC97L and MHCCLM3 stable nontarget control (CTL-KD) and NHE7 knockdown (NHE7-KD1, NHE7-KD3) clones and in HLE and PLC/PRF/5 stable vector control (CTL-SAM) and NHE7-overexpressing (NHE7-SAM1, NHE7-SAM2) clones. β -Actin was used as a loading control. Uptake of TMR-dextran (red) (C) and PKH67-sEV (green) in control and NHE7 knockdown cells (D). Uptake of TMR-dextran (red) (E) and PKH67-sEV (green) in control and NHE7 knockdown cells (F). DAPI staining marks nuclei (blue). Total particle per cell area was evaluated from at least five fields. At least 100 cells per experiment were analyzed. The fluorescent signal intensity was quantified and normalized to the respective control cells. Data are presented as the means \pm SEMs of 3 independent experiments. * $P < 0.05$; ** $P < 0.01$; *** $P < 0.001$. Abbreviations: CTL, ctrl; DAPI, 4',6-diamidino-2-phenylindole; HCC, hepatocellular carcinoma; KD, knockdown; NHE7, $\text{Na}^+(\text{+})/\text{H}^+(\text{+})$ exchanger 7; ns, non-significant; PCR, polymerase chain reaction; PKH67, Paul Karl Horan 67; SAM, synergistic activation mediator; SEMs, standard error of the means; sEV, small extracellular vesicle; TMR, tetramethyl rhodamine.

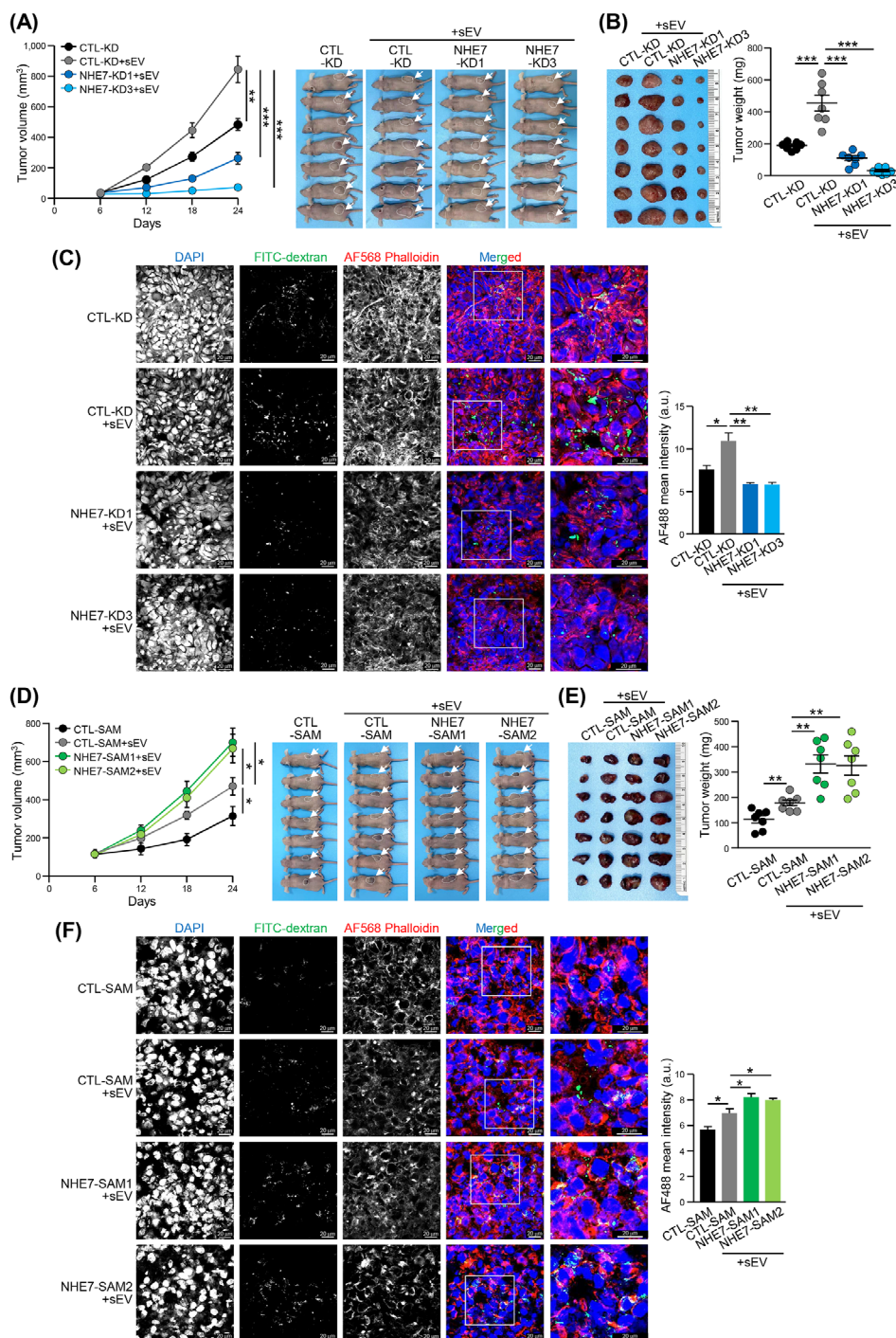


FIGURE 3 NHE7 promotes tumorigenesis induced by sEV uptake. (A) MHCC97L clones with stable NHE7 knockdown or nontargeting shRNA-expressing cells were subcutaneously co-injected with or without MHCCLM3-derived sEVs into nude mice. Tumor growth was monitored regularly. (B) Image and weight of tumors in the subcutaneous xenograft model at the experimental endpoint are shown ($n = 7$). (C) Visualization and quantification of macropinocytosis in vivo. Representative images from frozen sections of FITC-dextran (green)-injected tumor xenografts stained with phalloidin (red). DAPI staining (blue) marks nuclei. (D) Stable PLC/PRF/5 vector control and NHE7 overexpressing cells were subcutaneously co-injected with or without MHCCLM3-derived sEVs into nude mice. Tumor growth was measured regularly. (E) Image and weight of tumors in the subcutaneous xenograft model at the experimental endpoint are shown ($n = 7$). (F) Representative images from frozen sections of FITC-dextran (green)-injected tumor xenografts stained with phalloidin (red). DAPI staining (blue) marks nuclei. The intensity of FITC-dextran in 5 randomly selected fields was quantified. Data are presented as the means \pm SEMs. * $P < 0.05$; ** $P < 0.01$; *** $P < 0.001$. Abbreviations: AF, Alexa Fluor; CTL, ctrl; DAPI, 4',6-diamidino-2-phenylindole; FITC, fluorescein isothiocyanate; KD, knockdown; NHE7, Na(+)/H(+) exchanger 7; SAM, synergistic activation mediator; SEMs, standard error of the means; sEV, small extracellular vesicles.

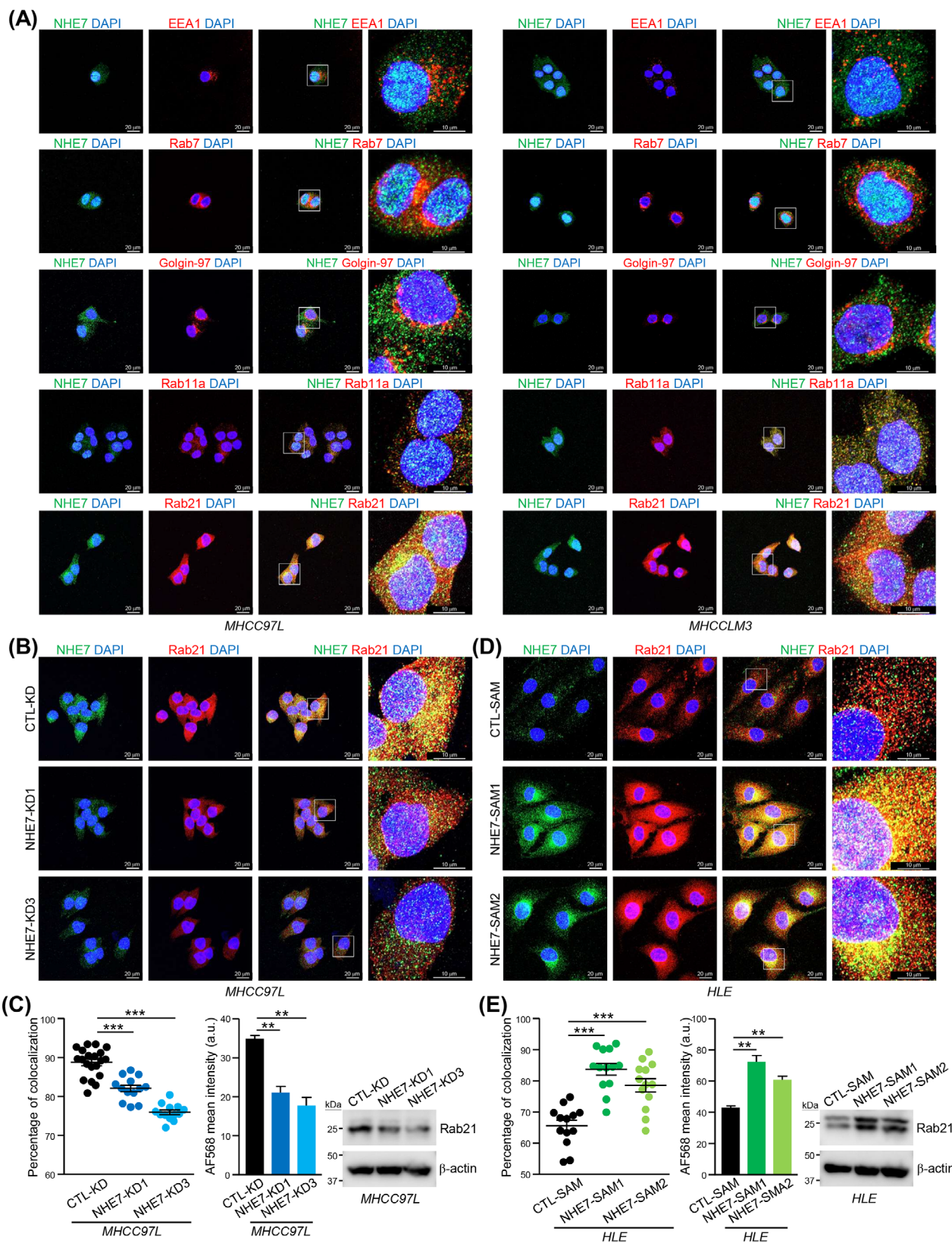


FIGURE 4 NHE7 co-localizes with Rab21 and promotes the maturation of macropinosomes. (A) Immunofluorescence staining of NHE7 (green), endosomal markers (red), EEA1, Rab7, Rab11a and Rab21, and the trans-Golgi network marker Golgin-97 in MHCC97L (left) and MHCCLM3 (right) cells. Cells were also stained with DAPI (blue). Coimmunofluorescence staining (B) and quantification (C) of NHE7 (green) and Rab21 (red) expression in MHCC97L nontargeting control (CTL-KD) and NHE7 knockdown (NHE7-KD) cells. HLE vector control (CTL-SAM) and NHE7-overexpressing (NHE7-SAM) cells were subjected to coimmunofluorescence staining (D) and the signal was analyzed

3.6 | NHE7-induced cytosolic alkalinity enhanced sEV uptake by macropinocytosis

NHE7 is a Na^+/H^+ exchanger that regulates pH levels [30]. We speculated that its function in regulation of intracellular pH determines the entry of sEVs into recipient cells by macropinocytosis. The pH indicator BCECF-AM was utilized to assess the pHi of cells, and it was found that the pHi of CTL-KD cells was higher than that of NHE7-KD cells, whereas the pHi was elevated in NHE7-SAM cells compared to CTL-SAM cells (Figure 5A). Cells were then subjected to a nigericin pH clamp technique (pH 6.5–8.5). Good linear relationships were identified between fluorescence ratio and intracellular pH in HCC cells (Supplementary Figure S9A). Consistent with the above findings, NHE7-KD cells exhibited delayed recovery of pHi changes induced by the NH_4Cl prepulse, and NHE7-SAM cells had a faster recovery of pHi (Figure 5B). To validate the pHi dependence of macropinocytosis, TMR-dextran and PKH67-sEV uptake was quantified in MHCC97L and MHCCLM3 cells in which the pHi was clamped at 6.5 and 7.5. The uptake of TMR-dextran and PKH67-sEV was significantly reduced in cells with a reduction in the pHi from 7.5 to 6.5 (Figure 5C). Accordingly, reduced sEV uptake led to a restrained capacity of cells to form colonies, migrate and invade (Supplementary Figure S10A). In contrast, overexpressing NHE7 impeded the inhibitory effect of acidification on TMR-dextran and PKH67-sEV uptake in NHE7-SAM cells (Figure 5D) and restored the growth and motility of cells at low pHi (Supplementary Figure S10B–C).

The acidic pH of the organellar lumen along endocytic pathways is a pivotal determinant for endosomal trafficking [35]. To investigate whether NHE7 modulates pHe in HCC cells, cells loaded with fluorescein tetramethylrhodamine-dextran were treated with nigericin and detected in pH-defined medium (pH 5.0–7.0) to analyze their fluorescence ratio (Supplementary Figure S9B). The results showed that NHE7 knockdown or overexpression increased or decreased the pHe, respectively (Figure 5E). The results agreed with earlier reports on the function of NHE7 as a proton-loading transporter in other cell types [30]. The pHe in NHE7-KD MHCC97L cells and NHE7-SAM HLE cells was significantly increased and decreased, respectively, upon treatment with monensin (Figure 5E). Collectively, these data showed that

the overexpressed NHE7 acts as a Na^+/H^+ exchanger to increase acidification and to promote the maturation of macropinosomes (Figure 5F).

3.7 | Blockade of NHE7 inhibited HCC growth and metastasis

The oncogenic role of NHE7 prompted us to test blockade of NHE7 as a treatment for HCC. We made use of Dox and IAA-induced inactivation of the NHE7 system to inhibit the expression of NHE7 in established tumors formed from NHE7-mAID-KO MHCC97L cells (Figure 6A and Supplementary Figure S11A). In a subcutaneous xenograft model, NHE7-mAID-KO MHCC97L cells efficiently promoted tumor formation compared to the parental cells, while Dox and IAA-induced inactivation of NHE7 markedly delayed tumor formation, resulting in tumors with reduced weight (Supplementary Figure S11B–D). Reduced NHE7 and Rab21 expression was found in tumors harvested from mice administered Dox and IAA (Supplementary Figure S11E). In a liver orthotopic implantation model, Dox and IAA-induced inactivation of NHE7 inhibited liver tumor growth and lung metastasis, as revealed by the weaker bioluminescence intensity in the harvested liver and lung tissues, respectively (Figure 6B–C). Histological analysis of lung tissues confirmed the lower number of metastases in the lungs and the reduced NHE7 and Rab21 expression in the tumors from mice treated with Dox and IAA (Figure 6D–F). The inhibition of tumorigenesis and metastasis was more prominent in mice co-treated with Dox, IAA and sorafenib compared to either NHE7 inhibition or sorafenib alone (Figure 6B–F). Macropinocytic activity was significantly compromised in tumors with reduced NHE7 expression harvested from mice treated with Dox and IAA compared to tumors formed in mice treated with vehicle (Figure 6G). These findings demonstrated the involvement of NHE7 in HCC and indicated that its blockade hinders HCC growth and distant metastasis.

3.8 | NHE7 was overexpressed and correlated with poor prognosis in HCC

As shown in Figure 7A, NHE7 upregulation was found in both paired and unpaired tumor tissues compared

(E) The percentage of NHE7 co-localized with Rab21 was quantified, and the mean AF568 fluorescence intensity was determined.

Immunoblotting was performed to evaluate Rab21 expression in MHCC97L and HLE cells. Data are presented as the means \pm SEMs.

** $P < 0.01$; *** $P < 0.001$. Abbreviations: AF, Alexa Fluor; CTL, ctrl; DAPI, 4',6-diamidino-2-phenylindole; EEA1, early endosome antigen 1; KD, knockdown; NHE7, Na^+/H^+ exchanger 7; Rab21, Ras-associated binding protein 21; SAM, synergistic activation mediator; SEMs, standard error of the means.

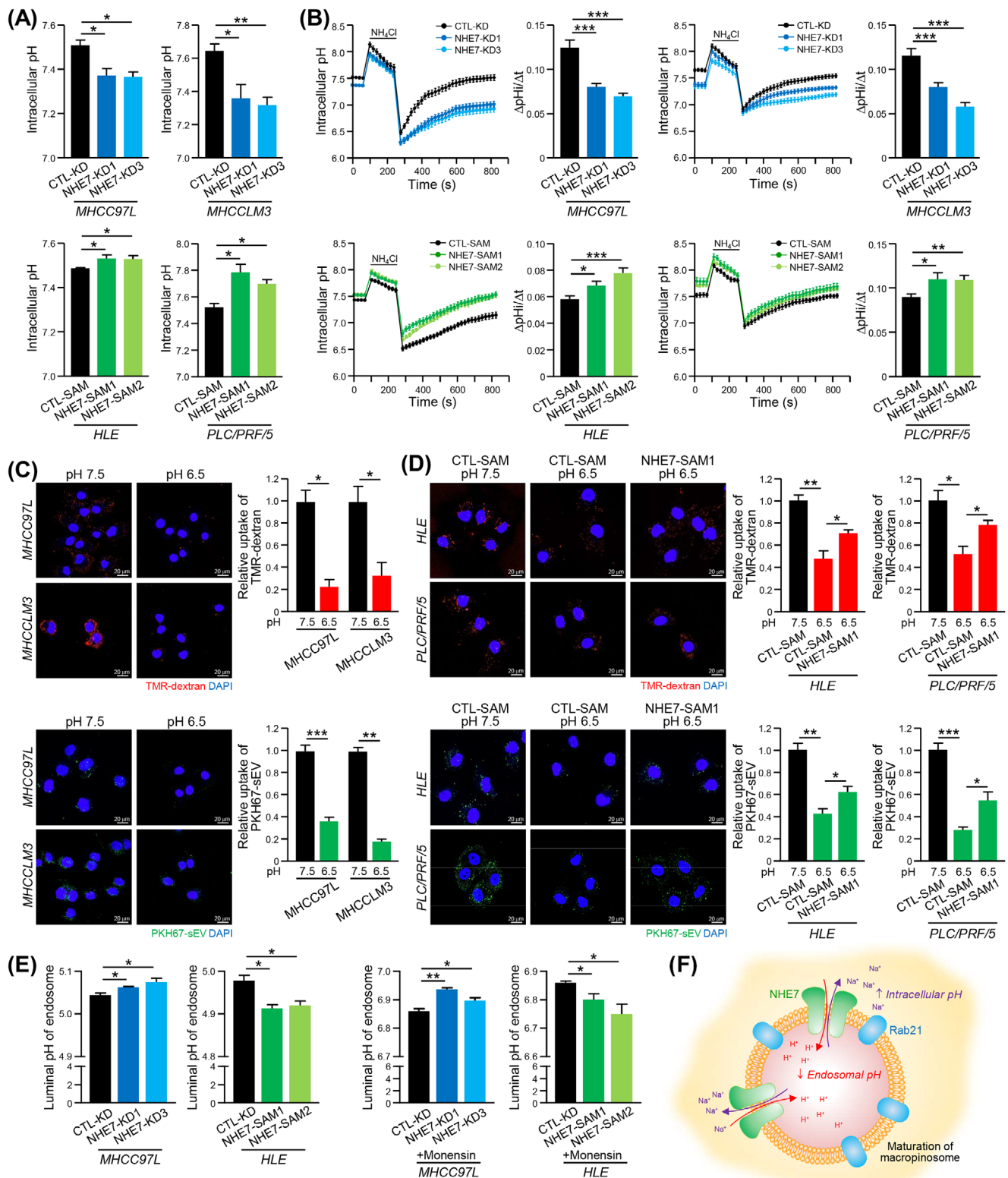


FIGURE 5 NHE7 increases intracellular pH, which facilitates the uptake of sEVs by macropinocytosis. (A) Determination of pHi in BCECF-loaded MHCC97L and MHCCCLM3 nontargeting control (CTL-KD) and NHE7 knockdown (NHE7-KD1, NHE7-KD3) stable clones (upper) and in HLE and PLC/PRF/5 vector control (CTL-SAM) and NHE7-overexpressing (NHE7-SAM1, NHE7-SAM2) stable clones (bottom). (B) Average tracings of the quantification of pHi recovery during an extracellular NH_4Cl pulse in BCECF-loaded NHE7 knockdown cells (upper) and NHE7-overexpressing cells (bottom). The recovery of pHi was calculated as $\Delta\text{pHi}/\Delta t$. (C) Quantification of TMR-dextran uptake (upper) and PKH67-sEV uptake (bottom) in MHCC97L and MHCCCLM3 pHi-clamped cells. (D) Quantification of TMR-dextran uptake (upper) and PKH67-sEV uptake (bottom) in HLE and PLC/PRF/5 CTL-SAM cells with the pHi clamped at 7.5 or 6.5 and in NHE7-SAM cells with the

to nontumor liver tissues. Patients with high NHE7 expression had worse prognoses than patients with low NHE7 expression (Figure 7B). We further examined whether the enhancement of macropinosome maturation by deregulated NHE7 is physiologically relevant. Multiplex immunofluorescence staining of NHE7 and Rab21 in a tissue microarray of 49 paired HCC and adjacent non-tumor liver tissues demonstrated that the levels of both NHE7 and Rab21 were markedly higher in tumor tissues (Figure 7C–D). A significant correlation between NHE7 and Rab21 expression was identified (Figure 7E). Taken together, our study experimentally demonstrated that NHE7, as a driver of macropinosome maturation, facilitates the internalization of sEVs by HCC cells, resulting in enhanced tumorigenesis and induction of metastasis. Mechanistically, NHE7 regulates intracellular and endosomal pH, which controls the internalization of sEVs (Figure 7F). Clinically, upregulation of NHE7 in HCC may predict poor prognosis in HCC.

4 | DISCUSSION

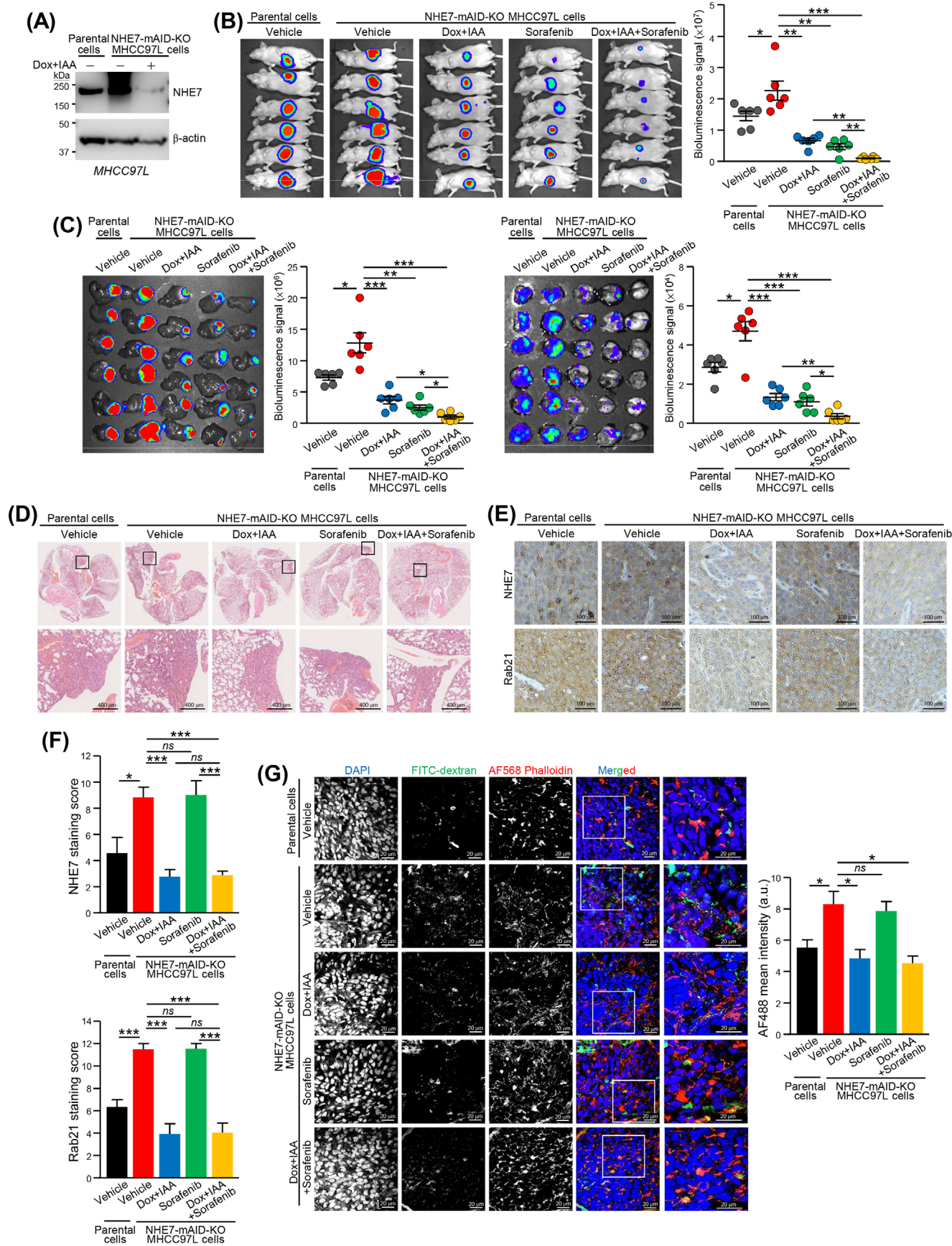
To date, few studies on the role of macropinocytosis in HCC have been reported. Under hypoxic conditions, macropinocytosis is induced by the elevation of EH domain-containing protein 2 expression to engulf extracellular nutrients for survival [36]. Macropinocytosis mediated by ATPase phospholipid transporting 9A (ATP9A) promotes nutrient starvation tolerance in HCC [37]. It has been shown to internalize and sort the C-X-C chemokine receptor type 4 (CXCR4) chemokine receptor to recycling endosomes [38]. Here, we further advanced the knowledge that macropinocytic activity gradually increases from non-metastatic HCC cells to metastatic HCC cells.

Our study delineates how NHE7 induces macropinocytosis by regulating intracellular pH. NHEs are categorized into plasma membrane-localized NHE1–5 and organellar NHE6–9, yet some NHEs are shuttling proteins localized in different subcellular compartments [39]. Here, we showed that NHE7 was localized at Rab21-positive mature macropinosomes. The level of Rab21 was positively reg-

ulated by NHE7, implicating the role of NHE7 in the maturation of macropinosomes. NHE7 also localizes to TGN [40]. It also binds caveolins, which are enriched in lipid rafts on the plasma membrane [41, 42]. This implies that NHE7 could be a shuttling protein localized in different subcellular compartments. NHE7 belongs to the SLC9 family, which encodes 13 distinct Na^+/H^+ exchanger orthologs. NHE7 mediates pH homeostasis in endosomes in a manner additive to that of V-ATPases and was found to accelerate endocytosis in astrocytes and lysosome biogenesis in a fibroblast line [23, 30]. NHE regulates ion and pH homeostasis by coupling the transfer of protons and counterflux of Na^+/K^+ across the membrane [40]. The cellular and organellar pH homeostasis that is controlled by Na^+/H^+ exchangers and vacuolar H^+ -ATPases is essential to the proper control of macropinocytosis [28, 43]. Microenvironmental pH has been reported to influence sEV release and uptake by cancer cells [44]. The acidity of the microenvironment influences cancer cells in different ways [45]. For example, extracellular acidosis promotes the metastatic ability of cancer cells. Parolini *et al.* [44] showed that low pH increased sEV release and uptake by melanoma cells. Cancer cells usually have higher intracellular pH than normal cells. In the endocytic pathway, the organellar pH gradually decreases in an inward direction, and the lysosomes are the most acidic organelles. The low pH provides a better environment for endosome maturation and function [35].

As NHEs are regulators of pH homeostasis, their deregulation highlights their potential role in human diseases. Our data showed that high NHE7 levels enhanced sEV uptake via macropinocytosis and promoted aggressive behaviors in metastatic HCC cells. This is in line with the functions of NHE7 in promoting the growth, invasiveness and tumorigenesis of invasive breast carcinoma cells [41] and pancreatic ductal adenocarcinoma cells [46]. The signaling pathway containing NHE7 has also been implicated in regulating CD8⁺ T-cell infiltration in breast cancer [47]. The clinical significance of NHE in HCC is largely unknown. Among all NHE family members, only NHE1 has been reported to be overexpressed in HCC [48, 49]. Using HCC data in the TCGA database and an in-house-constructed microarray of HCC tissues, we identified

pHi clamped at 6.5. Total particle per cell area was evaluated from at least five fields. At least 100 cells per experiment were analyzed. The fluorescent signal intensity was quantified and normalized to the respective control cells. (E) pH in dextran-positive endosomal compartments in MHCC97L CTL-KD and NHE7-KD cells and in HLE CTL-SAM and NHE7-SAM cells treated with (right) or without (left) monensin (500 mmol/L for 30 min). (F) Schematic diagram showing that NHE7 localizes at Rab21-positive endosomes, where it regulates the cytosolic and endosomal pH. Data are presented as the means \pm SEMs of 3 independent experiments. * P < 0.05; ** P < 0.01; *** P < 0.001. Abbreviations: BCECF, 2',7'-bis-(2-carboxyethyl)-5-(and-6)-carboxyfluorescein; CTL, ctrl; KD, knockdown; NHE7, Na^+/H^+ exchanger 7; pHi, intercellular pH; PKH67, Paul Karl Horan 67; Rab21, Ras-associated binding protein 21; SAM, synergistic activation mediator; SEMs, standard error of the means; sEVs, small extracellular vesicles; TMR, tetramethyl rhodamine.



that NHE7 was frequently elevated and linked to poor prognosis in HCC. The mechanistic pathway mediated by NHE7 in the promotion of macropinosome maturation indicated by Rab21 was also demonstrated to be physiologically

relevant. A significant correlation between NHE7 and Rab21 expression in HCC was shown in our analysis.

In addition to obtaining nutrients via macropinocytosis, tumor cells have been proved to actively uptake

FIGURE 6 Inducible inhibition of NHE7 alone and in combination with sorafenib shows inhibitory effects on HCC tumorigenesis and metastasis. (A) The expression of NHE7 in *NHE7*-mAID-KO MHCC97L cells with or without doxycycline (DOX, 2 mg/mL) and indole-3-acetic acid (IAA, 50 μ g/mL) treatment for 24 h was examined by immunoblotting. (B) Mice orthotopically injected with *NHE7*-mAID-KO MHCC97L cells were administered vehicle (DMSO), DOX (2 mg/mL in drinking water containing 5% sucrose), IAA (25 mg/kg/day) and sorafenib (30 mg/kg/day) for 2 weeks ($n = 6$). Bioluminescence imaging of whole mice was performed at the end of the experiment, and the signal intensity was quantified. (C) Ex vivo bioluminescence imaging of harvested livers (left) and lungs (right) is shown. The luciferase signals were quantified. (D) Representative images showing H&E staining of lung tissues. (E-F) Immunohistochemistry of NHE7 and Rab21 in liver tumor tissues. (G) Representative images of frozen sections of FITC-dextran (green)-injected liver tumors stained with phalloidin (red) and DAPI (blue). The histogram indicates the intensity of FITC-dextran in 5 randomly selected fields. Data are presented as the means \pm SEMs. * $P < 0.05$; ** $P < 0.01$; *** $P < 0.001$. Abbreviations: AF, Alexa Fluor; DAPI, 4',6-diamidino-2-phenylindole; DMSO, dimethyl sulfoxide; DOX, doxycycline; FITC, fluorescein isothiocyanate; HCC, hepatocellular carcinoma; IAA, indole-3-acetic acid; KO, knockout; mAID, mini-auxin-inducible degron; NHE7, Na(+)/H(+) exchanger 7; ns, non-significant; Rab21, Ras-associated binding protein 21; SEMs, standard error of the means.

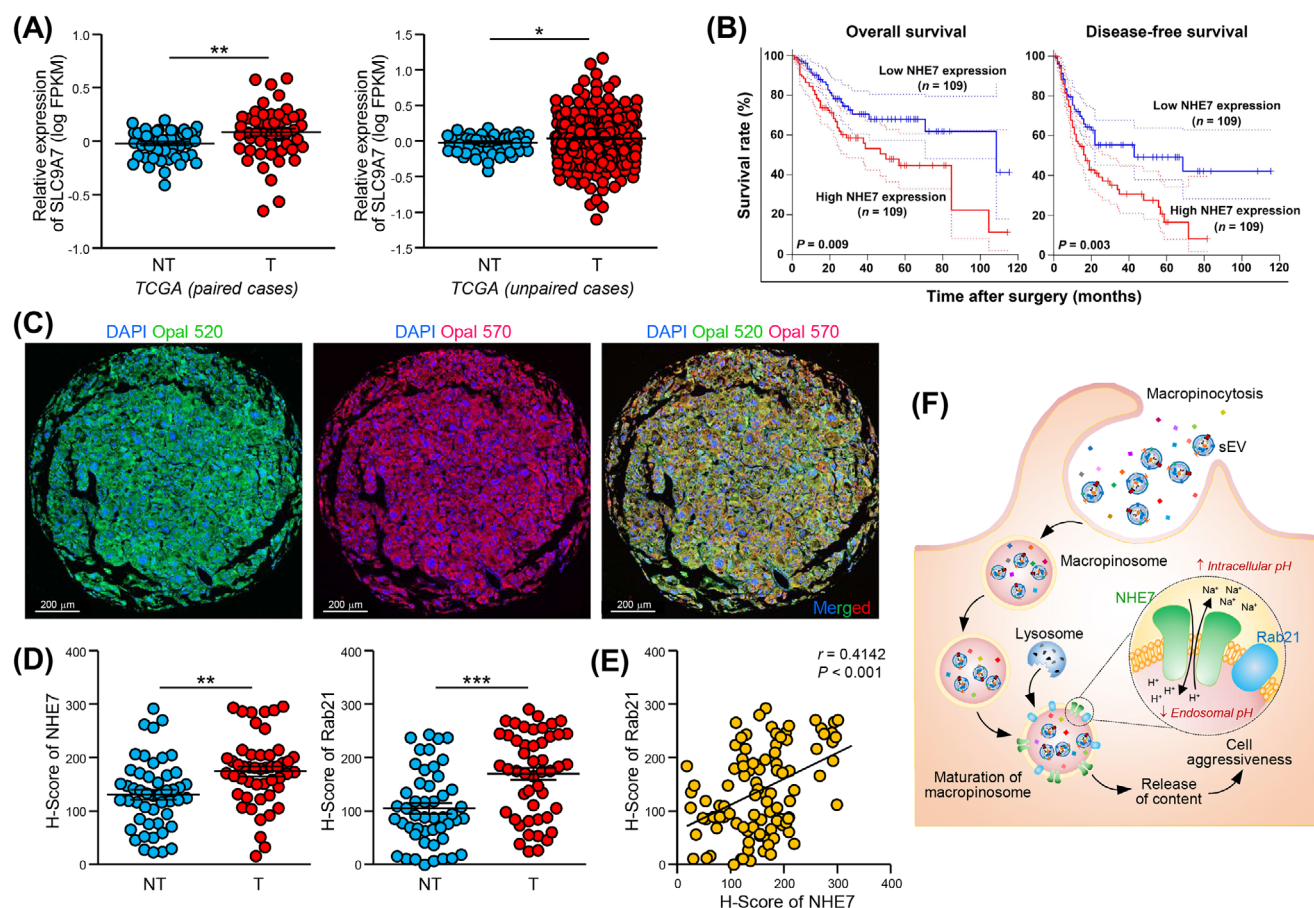


FIGURE 7 NHE7 expression and Rab21 expression are upregulated and correlated in HCC. (A) Analysis of NHE7 mRNA expression (SLC9A7) in paired ($n = 50$) and unpaired ($n = 370$) tumor and adjacent non-tumor liver tissues in an HCC cohort from the TCGA database. (B) Disease-free and overall survival of HCC patients with high and low levels of SLC9A7 expression. (C) Representative images of multiplex immunofluorescence staining, with nuclei in blue, NHE7 in green and Rab21 in red. (D) Signal intensities (H-scores) of NHE7 and Rab21 in tumor (T) and nontumor (NT) liver tissues. (E) The correlation of NHE7 and Rab21 expression was determined by Pearson correlation analysis. (F) Schematic representation of the proposed signaling pathway mediated by NHE7 in HCC. * $P < 0.05$; ** $P < 0.01$; *** $P < 0.001$. Abbreviations: HCC, hepatocellular carcinoma; H-score, histoscore; NHE7, Na(+)/H(+) exchanger 7; NT, nontumor; Rab21, Ras-associated binding protein 21; sEV, small extracellular vesicle; SLC9A7, solute carrier gene 9A7; T, tumor; TCGA, The Cancer Genome Atlas.

sEVs to modulate metabolism [50, 51]. It is beneficial for cancer cells to utilize macropinocytosis, and inhibition of macropinocytosis can therefore be envisioned as an anticancer therapeutic strategy. Indeed, dual blockade of autophagy and macropinocytosis limits nutrient and energy supply to cancer cells, leading to tumor regression [52]. In the present study, we identified that the inhibitory effect of targeting macropinocytosis led to the weakened cellular response to oncogenic sEVs. Macropinocytosis has been shown to be a negative regulator of ferroptosis and a contributing factor to sorafenib resistance in HCC [53]. Targeting sorafenib-induced macropinocytosis sensitizes tumors to sorafenib [53]. Dysfunction of NHEs has been associated with different diseases [54], and NHEs are potential targets for cancer therapies [55]. In agreement with these reported results, our results showed that inducible inhibition of NHE7-mediated macropinocytosis sensitized tumors to sorafenib treatment. Patients with advanced HCC are currently limited to receiving only palliative therapy. Based on our findings, blockade of sEV uptake via macropinocytosis can be a strategy to dampen the aggressive properties of metastatic advanced HCC.

There were still some limitations in this work. It is well recognized that HCC develops on a chronic liver disease with different etiology including chronic viral infection, alcoholic cirrhosis, non-alcoholic fatty liver diseases or autoimmune liver disease [56]. In the current study, the relationship between different etiologies of HCC and macropinocytosis was not functionally evaluated. Nevertheless, the clinical samples adopted in the tissue microarray were mostly obtained from patients with chronic hepatitis B infection, implicating the clinical relevance of the upregulation of NHE7 and Rab21 and the potential impact of macropinocytosis in HCC with the underlying disease of hepatitis B infection. Accumulating studies demonstrated tyrosine kinase inhibitor, regorafenib, as a potential therapeutic strategy for HCC patients who has no option of curative surgery [57]. Furthermore, emerging systemic treatments based on the combination of tyrosine kinase inhibitor with immune checkpoint inhibitor have indication of good synergistic antitumor efficacy for HCC [58]. Whether NHE7 has a good combined effect with other tyrosine kinase inhibitors or immune checkpoint inhibitor is worthy of investigation in the future study.

5 | CONCLUSIONS

In summary, we identified that high NHE7 expression enhanced sEV uptake by macropinocytosis and pro-

moted the malignant properties of HCC cells. Mechanistically, NHE7 regulated intracellular and endosomal pH, which promoted macropinocytosis and the maturation of macropinosomes, respectively. The expression of Rab21, a marker of mature macropinosomes, was shown to be positively correlated with that of NHE7 in HCC tissues, suggesting the physiological relevance of the mechanistic pathway mediated by NHE7 in HCC. In view of the unfavorable prognosis of HCC, the present study highlighted the potential of developing anti-NHE7 therapeutics. Inducible disruption of NHE7 expression in established tumors alone or combined with sorafenib administration resulted in diminished tumor development, suggesting that NHE7 is a promising therapeutic target of HCC. These results uncovered the mechanism by which NHE7 attenuated HCC progression via interfering macropinocytic activity, unveiling a prospective therapeutic target for advanced HCC.

DECLARATIONS

AUTHOR CONTRIBUTIONS

Conceptualization: JWPY; Vectors Construction: YY, HTM, YX; In vitro Functional Experiments: YY; Immunofluorescence Assay: YY, TX, ZX, PT, HLF; Animal Experiments: YY, YX, LY; Data Curation: YY, JWPY; Resources: JPY; Writing-Original Draft: YY, XY; Writing-Review & Editing: JWPY; Supervision: JWPY; Funding Acquisition: YX, JWPY.

ACKNOWLEDGEMENTS

We acknowledge the In Vivo Imaging System and confocal microscope supplied by Imaging and Flow Cytometry Core at the Centre for PanorOmic Sciences, Li Ka Shing Faculty of Medicine, The University of Hong Kong (Hong Kong, China). We also thank Centre for Comparative Medicine Research for providing animals and facility for animal experimentation and the Electron Microscope Unit for providing service and support needed for experiments involving electron microscope. The work was funded by Research Grants Council General Research Fund (Grant No. 17105322), Hong Kong Scholars Program (Grant No. XJ2020012 and 2020-036), University Research Committee Seed Fund for Basic Research (Grant No. 202111159009) of The University of Hong Kong, Marshal Initiative Funding of Harbin Medical University (Grant No. HMUMIF-22008), Open Funds of State Key Laboratory of Oncology in South China (Grant No. HN2023-02), and Natural Science Foundation of Heilongjiang Province (Grant No. LH2023H043).

ETHICS APPROVAL AND CONSENT TO PARTICIPATE

Approval for the use of clinical samples was obtained from the Ethics Committee of Sun Yat-sen University Cancer Center (B2021-459-01) and the University of Hong Kong (UW 11-448). Informed consents were acquired from patients. The animal experiments were performed under the research protocol (CULATR 5925-21) approved by Committee of the Use of Live Animals in Teaching and Research, The University of Hong Kong.

CONSENT FOR PUBLICATION

Not applicable.


CONFLICT OF INTEREST STATEMENT

The authors declare no conflict of interest.

DATA AVAILABILITY STATEMENT

The data that support the findings of this study are available from the corresponding author upon reasonable request.

ORCID

Judy Wai Ping Yam  <https://orcid.org/0000-0002-5637-121X>

REFERENCES

- Llovet JM, Kelley RK, Villanueva A, Singal AG, Pikarsky E, Roayaie S, et al. Hepatocellular carcinoma. *Nat Rev Dis Primers*. 2021;7(1):6.
- Becker A, Thakur BK, Weiss JM, Kim HS, Peinado H, Lyden D. Extracellular Vesicles in Cancer: Cell-to-Cell Mediators of Metastasis. *Cancer Cell*. 2016;30(6):836-848.
- Mao X, Tey SK, Yeung CLS, Kwong EML, Fung YME, Chung CYS, et al. Nidogen 1-enriched extracellular vesicles facilitate extrahepatic metastasis of liver cancer by activating pulmonary fibroblasts to secrete tumor necrosis factor receptor 1. *Adv Sci (Weinh)*. 2020;7(21):2002157.
- Tey SK, Wong SWK, Chan JYT, Mao X, Ng TH, Yeung CLS, et al. Patient pIgR-enriched extracellular vesicles drive cancer stemness, tumorigenesis and metastasis in hepatocellular carcinoma. *J Hepatol*. 2022;76(4):883-895.
- Hou PP, Luo LJ, Chen HZ, Chen QT, Bian XL, Wu SF, et al. Ectosomal PKM2 Promotes HCC by Inducing Macrophage Differentiation and Remodeling the Tumor Microenvironment. *Mol Cell*. 2020;78(6):1192-1206.e1110.
- Mulcahy LA, Pink RC, Carter DR. Routes and mechanisms of extracellular vesicle uptake. *J Extracell Vesicles*. 2014;3.
- Fujii M, Kawai K, Egami Y, Araki N. Dissecting the roles of Rac1 activation and deactivation in macropinocytosis using microscopic photo-manipulation. *Sci Rep*. 2013;3:2385.
- Commisso C, Davidson SM, Soydaner-Azeloglu RG, Parker SJ, Kamphorst JJ, Hackett S, et al. Macropinocytosis of protein is an amino acid supply route in Ras-transformed cells. *Nature*. 2013;497(7451):633-637.
- Kim SM, Nguyen TT, Ravi A, Kubiniok P, Finicle BT, Jayashankar V, et al. PTEN deficiency and AMPK activation promote nutrient scavenging and anabolism in prostate cancer cells. *Cancer Discov*. 2018;8(7):866-883.
- Mayers JR, Torrence ME, Danai LV, Papagiannakopoulos T, Davidson SM, Bauer MR, et al. Tissue of origin dictates branched-chain amino acid metabolism in mutant Kras-driven cancers. *Science*. 2016;353(6304):1161-1165.
- Costa Verdera H, Gitz-Francois JJ, Schiffelers RM, Vader P. Cellular uptake of extracellular vesicles is mediated by clathrin-independent endocytosis and macropinocytosis. *J Control Release*. 2017;266:100-108.
- Kamkar S, LeBleu VS, Sugimoto H, Yang S, Ruivo CF, Melo SA, et al. Exosomes facilitate therapeutic targeting of oncogenic KRAS in pancreatic cancer. *Nature*. 2017;546(7659):498-503.
- Li X, Chen R, Kemper S, Brigstock DR. Structural and functional characterization of fibronectin in extracellular vesicles from hepatocytes. *Front Cell Dev Biol*. 2021;9:640667.
- Wei JX, Lv LH, Wan YL, Cao Y, Li GL, Lin HM, et al. Vps4A functions as a tumor suppressor by regulating the secretion and uptake of exosomal microRNAs in human hepatoma cells. *Hepatology*. 2015;61(4):1284-1294.
- Song S, Zhang Y, Ding T, Ji N, Zhao H. The dual role of macropinocytosis in cancers: Promoting growth and inducing methuosis to participate in anticancer therapies as targets. *Front Oncol*. 2020;10:570108.
- Yeung TK, Lau HW, Ma HT, Poon RYC. One-step multiplex toolkit for efficient generation of conditional gene silencing human cell lines. *Mol Biol Cell*. 2021;32(14):1320-1330.
- Motohashi K. A simple and efficient seamless DNA cloning method using SLiCE from *Escherichia coli* laboratory strains and its application to SLiP site-directed mutagenesis. *BMC Biotechnol*. 2015;15:47.
- Fennell M, Commisso C, Ramirez C, Garippa R, Bar-Sagi D. High-content, full genome siRNA screen for regulators of oncogenic HRAS-driven macropinocytosis. *Assay Drug Dev Technol*. 2015;13(7):347-355.
- Tomayko MM, Reynolds CP. Determination of subcutaneous tumor size in athymic (nude) mice. *Cancer Chemother Pharmacol*. 1989;24(3):148-154.
- Lee SW, Alas B, Commisso C. Detection and quantification of macropinosomes in pancreatic tumors. *Methods Mol Biol*. 2019;1882:171-181.
- Francisco-Cruz A, Parra ER, Tetzlaff MT, Wistuba II. Multiplex immunofluorescence assays. *Methods Mol Biol*. 2020;2055:467-495.
- Ozkan P, Mutharasan R. A rapid method for measuring intracellular pH using BCECF-AM. *Biochim Biophys Acta*. 2002;1572(1):143-148.
- Lopez-Hernandez T, Puchkov D, Krause E, Maritzen T, Haucke V. Endocytic regulation of cellular ion homeostasis controls lysosome biogenesis. *Nat Cell Biol*. 2020;22(7):815-827.
- Nakanishi T, Gu H, Seguchi M, Cragoe EJ, Jr., Momma K. HCO₃⁻-dependent intracellular pH regulation in the premature myocardium. *Circ Res*. 1992;71(6):1314-1323.
- van Weert AW, Dunn KW, Geuze HJ, Maxfield FR, Stoorvogel W. Transport from late endosomes to lysosomes, but not sorting of integral membrane proteins in endosomes, depends on the vacuolar proton pump. *J Cell Biol*. 1995;130(4):821-834.

26. Tang Z, Li C, Kang B, Gao G, Li C, Zhang Z. GEPIA: a web server for cancer and normal gene expression profiling and interactive analyses. *Nucleic Acids Res.* 2017;45(W1):W98-W102.
27. Ivanov AI. Pharmacological inhibition of endocytic pathways: is it specific enough to be useful? *Methods Mol Biol.* 2008;440:15-33.
28. Koivusalo M, Welch C, Hayashi H, Scott CC, Kim M, Alexander T, et al. Amiloride inhibits macropinocytosis by lowering submembranous pH and preventing Rac1 and Cdc42 signaling. *J Cell Biol.* 2010;188(4):547-563.
29. Cosson P, de Curtis I, Pouyssegur J, Griffiths G, Davoust J. Low cytoplasmic pH inhibits endocytosis and transport from the trans-Golgi network to the cell surface. *J Cell Biol.* 1989;108(2):377-387.
30. Milosavljevic N, Monet M, Lena I, Brau F, Lacas-Gervais S, Feliciangeli S, et al. The intracellular Na⁽⁺⁾/H⁽⁺⁾ exchanger NHE7 effects a Na⁽⁺⁾-coupled, but not K⁽⁺⁾-coupled proton-loading mechanism in endocytosis. *Cell Rep.* 2014;7(3):689-696.
31. Mu FT, Callaghan JM, Steele-Mortimer O, Stenmark H, Parton RG, Campbell PL, et al. EEA1, an early endosome-associated protein. EEA1 is a conserved alpha-helical peripheral membrane protein flanked by cysteine "fingers" and contains a calmodulin-binding IQ motif. *J Biol Chem.* 1995;270(22):13503-13511.
32. Zhang J, Zhang X, Liu G, Chang D, Liang X, Zhu X, et al. Intracellular Trafficking Network of Protein Nanocapsules: Endocytosis, Exocytosis and Autophagy. *Theranostics.* 2016;6(12):2099-2113.
33. Derby MC, van Vliet C, Brown D, Luke MR, Lu L, Hong W, et al. Mammalian GRIP domain proteins differ in their membrane binding properties and are recruited to distinct domains of the TGN. *J Cell Sci.* 2004;117(Pt 24):5865-5874.
34. Egami Y, Araki N. Dynamic changes in the spatiotemporal localization of Rab21 in live RAW264 cells during macropinocytosis. *PLoS One.* 2009;4(8):e6689.
35. Huotari J, Helenius A. Endosome maturation. *EMBO J.* 2011;30(17):3481-3500.
36. Zhang MS, Cui JD, Lee D, Yuen VW, Chiu DK, Goh CC, et al. Hypoxia-induced macropinocytosis represents a metabolic route for liver cancer. *Nat Commun.* 2022;13(1):954.
37. Wang X, Li Y, Xiao Y, Huang X, Wu X, Zhao Z, et al. The phospholipid flippase ATP9A enhances macropinocytosis to promote nutrient starvation tolerance in hepatocellular carcinoma. *J Pathol.* 2023;260(1):17-31.
38. Cepeda EB, Dediulia T, Fernando J, Bertran E, Egea G, Navarro E, et al. Mechanisms regulating cell membrane localization of the chemokine receptor CXCR4 in human hepatocarcinoma cells. *Biochim Biophys Acta.* 2015;1853(5):1205-1218.
39. Donowitz M, Ming Tse C, Fuster D. SLC9/NHE gene family, a plasma membrane and organellar family of Na⁽⁺⁾/H⁽⁺⁾ exchangers. *Mol Aspects Med.* 2013;34(2-3):236-251.
40. Numata M, Orlowski J. Molecular cloning and characterization of a novel (Na⁺,K⁺)/H⁺ exchanger localized to the trans-Golgi network. *J Biol Chem.* 2001;276(20):17387-1794.
41. Onishi I, Lin PJ, Numata Y, Austin P, Cipollone J, Roberge M, et al. Organellar (Na⁺, K⁺)/H⁺ exchanger NHE7 regulates cell adhesion, invasion and anchorage-independent growth of breast cancer MDA-MB-231 cells. *Oncol Rep.* 2012;27(2):311-3417.
42. Lin PJ, Williams WP, Kobiljski J, Numata M. Caveolins bind to (Na⁺, K⁺)/H⁺ exchanger NHE7 by a novel binding module. *Cell Signal.* 2007;19(5):978-988.
43. Ramirez C, Hauser AD, Vucic EA, Bar-Sagi D. Plasma membrane V-ATPase controls oncogenic RAS-induced macropinocytosis. *Nature.* 2019;576(7787):477-841.
44. Parolini I, Federici C, Raggi C, Lugini L, Palleschi S, De Milito A, et al. Microenvironmental pH is a key factor for exosome traffic in tumor cells. *J Biol Chem.* 2009;284(49):34211-34222.
45. Boedtker E, Pedersen SF. The acidic tumor microenvironment as a driver of cancer. *Annu Rev Physiol.* 2020;82:103-126.
46. Galenkamp KMO, Sosicka P, Jung M, Recouvreur MV, Zhang Y, Moldenhauer MR, et al. Golgi acidification by NHE7 regulates cytosolic pH homeostasis in pancreatic cancer cells. *Cancer Discov.* 2020;10(6):822-835.
47. Wang Z, Yang X, Shen J, Xu J, Pan M, Liu J, et al. Gene expression patterns associated with tumor-infiltrating CD4⁺ and CD8⁺ T cells in invasive breast carcinomas. *Hum Immunol.* 2021;82(4):279-287.
48. Yang X, Wang D, Dong W, Song Z, Dou K. Expression and modulation of Na⁽⁺⁾/H⁽⁺⁾ exchanger 1 gene in hepatocellular carcinoma: A potential therapeutic target. *J Gastroenterol Hepatol.* 2011;26(2):364-370.
49. Yang X, Wang D, Dong W, Song Z, Dou K. Over-expression of Na⁺/H⁺ exchanger 1 and its clinicopathologic significance in hepatocellular carcinoma. *Med Oncol.* 2010;27(4):1109-1113.
50. Zhao H, Yang L, Baddour J, Achreja A, Bernard V, Moss T, et al. Tumor microenvironment derived exosomes pleiotropically modulate cancer cell metabolism. *Elife.* 2016;5:e10250.
51. Nakase I, Kobayashi NB, Takatani-Nakase T, Yoshida T. Active macropinocytosis induction by stimulation of epidermal growth factor receptor and oncogenic Ras expression potentiates cellular uptake efficacy of exosomes. *Sci Rep.* 2015;5:10300.
52. Su H, Yang F, Fu R, Li X, French R, Mose E, et al. Cancer cells escape autophagy inhibition via NRF2-induced macropinocytosis. *Cancer Cell.* 2021;39(5):678-693 e611.
53. Byun JK, Lee S, Kang GW, Lee YR, Park SY, Song IS, et al. Macropinocytosis is an alternative pathway of cysteine acquisition and mitigates sorafenib-induced ferroptosis in hepatocellular carcinoma. *J Exp Clin Cancer Res.* 2022;41(1):98.
54. Fuster DG, Alexander RT. Traditional and emerging roles for the SLC9 Na⁺/H⁺ exchangers. *Pflugers Arch.* 2014;466(1):61-76.
55. Stock C, Pedersen SF. Roles of pH and the Na⁽⁺⁾/H⁽⁺⁾ exchanger NHE1 in cancer: From cell biology and animal models to an emerging translational perspective? *Semin Cancer Biol.* 2017;43:5-16.
56. Jindal A, Thadi A, Shailubhai K. Hepatocellular carcinoma: Etiology and current and future drugs. *J Clin Exp Hepatol.* 2019;9(2):221-232.
57. Granito A, Marinelli S, Forgione A, Renzulli M, Benevento F, Piscaglia F, et al. Regorafenib combined with other systemic therapies: exploring promising therapeutic combinations in HCC. *J Hepatocell Carcinoma.* 2021;8:477-492.
58. Stefanini B, Ielasi L, Chen R, Abbati C, Tonnini M, Tovoli F, et al. TKIs in combination with immunotherapy for

hepatocellular carcinoma. *Expert Rev Anticancer Ther.* 2023;23(3):279-291.

SUPPORTING INFORMATION

Additional supporting information can be found online in the Supporting Information section at the end of this article.

How to cite this article: Yao Y, Xu Y, Yu L, Xue T-M, Xiao Z-J, Tin P-C, et al. NHE7 upregulation potentiates the uptake of small extracellular vesicles by enhancing maturation of macropinosomes in hepatocellular carcinoma. *Cancer Commun.* 2024;44:251–272. <https://doi.org/10.1002/cac2.12515>